

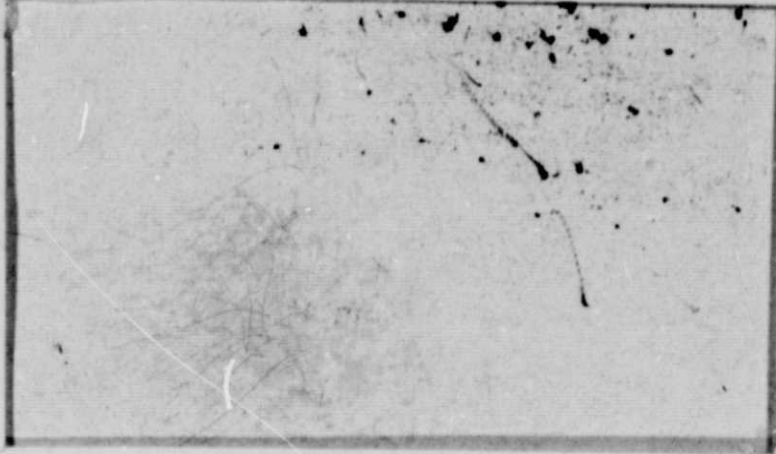
General Disclaimer

One or more of the Following Statements may affect this Document

- This document has been reproduced from the best copy furnished by the organizational source. It is being released in the interest of making available as much information as possible.
- This document may contain data, which exceeds the sheet parameters. It was furnished in this condition by the organizational source and is the best copy available.
- This document may contain tone-on-tone or color graphs, charts and/or pictures, which have been reproduced in black and white.
- This document is paginated as submitted by the original source.
- Portions of this document are not fully legible due to the historical nature of some of the material. However, it is the best reproduction available from the original submission.

NASA CR-152593

NAS5-23479



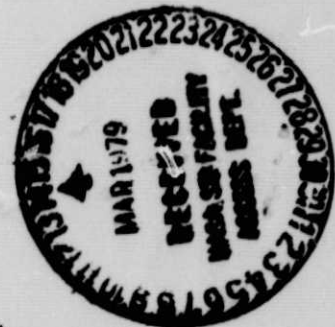
(NASA-CR-152593) STUDY OF LARGE ADAPTIVE
ARRAYS FOR SPACE TECHNOLOGY APPLICATIONS
Final Report, 27 Apr. 1976 - 26 Apr. 1977
(Pennsylvania Univ.) 107 p HC A06/MF A01

N79-18158

Unclas
16137
CSCL 20N G3/32



ORIGINAL PAGE IS
OF POOR QUALITY



UNIVERSITY of PENNSYLVANIA
VALLEY FORGE RESEARCH CENTER
THE MOORE SCHOOL OF ELECTRICAL ENGINEERING
PHILADELPHIA, PENNSYLVANIA 19174



TABLE OF CONTENTS

1.	INTRODUCTION	1
2.	ARRAY-IN-SPACE SYSTEM CONCEPT DEVELOPMENT	7
	2.1 GENERAL OBJECTIVES	7
	2.2 FIRST SYSTEM CONCEPT: Self-Cohering Radio Camera	10
	2.3 SECOND SYSTEM CONCEPT: Self-Survey Radio Camera	22
	2.3.1 ARRAY ELEMENTS SURVEY	23
	2.3.2 SOURCE POSITION LOCATION ALGORITHM	28
	2.3.3 ELECTRONIC SYSTEM CONSIDERATIONS	32
	2.4 THIRD SYSTEM CONCEPT: THE SIMULTANEOUS TRANSFORM ARRAY	43
	2.4.1 EARTH VIEWING RADAR	47
	2.4.2 RADIO TELESCOPE FOR DEEP SPACE	51
3.	ATS-6 TO EARTH SPATIAL CORRELATION EXPERIMENT AT L-BAND	55
	3.1 THE EXPERIMENT	55
	3.2 RESULTS	59
	3.3 THEORETICAL INVESTIGATION	64
	3.4 OBSERVATIONS	70
4.	SUMMARY AND CONCLUSIONS	74
5.	RECOMMENDATIONS FOR FUTURE WORK	76
6.	REFERENCES	78
7.	APPENDICES I through VII	
	APPENDIX I:	80
	Relations Between Pointing Angles from a Spaceborne Array and the Positions on the Earth's Surface	
	APPENDIX II:	87
	Dependence of the Uncertainty in Angular Location on the Bandwidth of the System	
	APPENDIX III:	90
	Tolerance on Element Location Uncertainty for Scanning in Space and in Frequency	
	APPENDIX IV:	94
	Array Bandwidth	
	APPENDIX V:	99
	Location of Random Array Elements Using Phase Measurements	
	APPENDIX VI: Sample Signal Power Calculation	104
	APPENDIX VII: Differential Phase Calculation	105

STUDY OF LARGE ADAPTIVE ARRAYS
FOR SPACE TECHNOLOGY APPLICATIONS

Raymond S. Berkowitz
Bernard D. Steinberg
Yakov Shamash
Earl N. Powers
Tong L. Lim

Final Report Submitted to
National Aeronautics and Space Administration
Goddard Space Flight Center
Greenbelt, Maryland 20771

Contract No: NAS 5-23479
Duration: 4/27/76-4/26/77

Principal Investigator: Raymond S. Berkowitz

Valley Forge Research Center
The Moore School of Electrical Engineering
University of Pennsylvania
Philadelphia, Pennsylvania

ABSTRACT

The general objective of this project was to perform research in large adaptive antenna arrays for space technology applications. Specifically two tasks were considered. The first was a system design study for accurate determination of the positions and the frequencies of sources radiating from the earth's surface that could be used for the rapid location of people or vehicles in distress. This system design study led to a nonrigid array about 8 km in size with means for locating the array element positions, receiving signals from the earth and determining the source locations and frequencies of the transmitting sources. It was concluded that this system design is feasible, and satisfies the desired objectives.

The second task was an experiment to determine the largest earthbound array which could simulate a spaceborne experiment. It was determined that an 800 ft array would perform indistinguishably in both locations and it is estimated that one several times larger also would serve satisfactorily. In addition the power density spectrum of the phase difference fluctuations across a large array was measured. It was found that the spectrum falls off approximately as $f^{-5/2}$.

STUDY OF LARGE ADAPTIVE ARRAYS
FOR SPACE TECHNOLOGY APPLICATIONS

1. INTRODUCTION

High angular measurement accuracy and resolution implies large aperture. The resolution of an imaging device is in the order of the reciprocal of the number of wavelengths across the aperture. Thus a five cm lens, which is 10^5 optical wavelengths in diameter, has a potential resolving power of 10^{-5} radians. There are many applications for which optical wavelength electromagnetic waves are not appropriate. Clouds and rain which can be penetrated easily by radio waves are essentially impenetrable to optical waves.

Since microwaves are much longer than optical waves, a system which uses these waves to realize a resolution equal to that of an optical instrument must possess an extremely large aperture. Most current radars operate with microwave wavelengths in the range from 3 cm (X-band) to 30 cm (L-band). The size of a microwave aperture with a resolution of 10^{-5} radians would be 3 to 30 kms.

Large aperture systems introduce fundamental problems. Microwave dishes larger than a few hundred feet are usually impractical because of distortions resulting from gravitational and thermal stresses. Furthermore, the silhouette of a large dish makes it impractical for certain environments. The phased array is a legitimate approach to achieving a large aperture without imposing the mechanical and silhouette problems of the microwave dish.

Conventional phased array design, however, is totally inappropriate for a giant structure, for the following reasons:

- (i) Conventional phased array design requires that antenna elements be spaced on the order of one-half wavelength. Thus achievement of 10^{-5} beamwidth would require more than 10^{10} elements, which is intolerably costly.
- (ii) Conventional phased array design requires a planar surface which is impractical for very large arrays.
- (iii) When the aperture exceeds some size, which is a function of the wavelength, the practicality of surveying the position of the parts of the array to the required $1/10$ of a wavelength decreases rapidly.
- (iv) Large structures, such as ships and aircraft and large space vehicles are nonrigid, requiring a dynamic measurement of and compensation for the time varying coordinates of each antenna element to an accuracy of $1/10$ of a wavelength.

A minimum approach to the solution of these fundamental problems is to thin the array so that no more than the order of 1000 elements, say are required independently of the size of the aperture. The elements are distributed randomly through the aperture so as to eliminate the grating lobes which normally would result from a thinned aperture. The array can be made to conform with whatever surface is involved. In the current design another order of magnitude of thinning can be accomplished because of certain restrictions in the demands upon the system.

The work reported herein is a natural extension of the general research program of the Valley Forge Research Center. The central theme of

this work is the development of techniques by which large, nonrigid antenna arrays may be used to operate in turbulent transmission media. The basic concept is that of reflecting radiated energy from a remote target, sensing the back-scattered radiation via an array of antenna elements which are scattered randomly over some surface or through some volume, then processing the received signals to form a high resolution image of the target. Such a system is referred to as a radio camera.

The required technological innovations associated with the radio camera fall primarily in the area of adaptive operation of large, random, thin, conformal arrays. Fundamental research is being carried out in adaptive space-time signal processing; adaptive nulling; multipath suppression; optimization of image quality on the basis of feedback from the image; phase measurement techniques; angular measurement techniques; and signal parameter estimation in the presence of noise, clutter, and propagation anomalies.

Potential applications of the radio camera are many: airspace, ocean surface, underwater or ground surveillance for military or civilian purposes (ground based, floating, airborne or satellite), high angular resolution imaging of internal organs in medicine, seismics, and meteorological measurement.

To this end, the NASA sponsored work (to be described in this report) was a first examination of the potential of the radio camera in space. In particular the design deals with a large spaceborne array with many elements randomly located in a near-planar surface for the formation of high angular resolution beams. The purposes of the array were:

- (a) The location of a disabled air or surface vehicle in distress by direction finding on a microwave emergency emission from the vehicle.
- (b) Multiple frequency high angular resolution beam-forming for communicating with multiple ground sources and/or monitoring sources of radio interference.

The work for this project was divided into two tasks as follows:

Task 1: Design of self-cohering microwave system for high resolution beamforming and location of signal sources.

Task 2: Conduct a spatial correlation experiment to determine propagation limitations to the performance and useful size of a large, conformal array on the surface of the earth.

Task 1 was concerned with identifying technology that may be useful in the application of large spaceborne as well as earthbound arrays. Task 2 was concerned with determination of spatial correlation of L-band signals received on the ground from a transmission from a geosynchronous satellite (ATS-6).

For task 1, three system concepts have been developed. The first system concept was based on the use of fixed references on the earth's surface to synchronize a randomly distributed antenna array which is in geostationary orbit. Once synchronized, the array scans the region in the neighborhood of the synchronizing source to locate any other sources which may be present. Even though the concept proved to be theoretically and physically sound, its world-wide implementation was found to be impractical, since it required the ability to place beacons uniformly on the earth's surface which for geo-political reasons is unacceptable. Thus the second

system concept was developed. In this concept it is assumed that an element location subsystem can be created consisting of beacons clustered on the land masses and distributed over the earth. Given that assumption, it is only necessary that each array module in the spaceborne system be able to measure the phase of the radiation field at sufficiently frequent intervals and transmit this information to the earth. The complex samples and the locations from which the samples were taken constitute the only information required by a signal processor to locate the angular coordinates of the source or sources. The "space" system essentially consists of three parts. The first is concerned with the surveying procedure to be used for locating the positions of the elements of the spaceborne array. The second part consists of the electrical hardware requirements, while the third part is concerned with actual location and identification of distress signals from the earth's surface.

A surveying algorithm has been derived which is based on the use of phase measurements at the antenna elements of signals transmitted by a set of well determined randomly distributed beacons on the earth's surface. The element positions so computed are unique for the given set of phase measurements. The tolerances on element location, beacon positions and frequency have been calculated and found to completely satisfy the system specifications. It has been shown that the same algorithm may also be used for locating and identifying distress signals, thereby solving also the third part of the design problem.

As for the electrical system, analysis was focused on the use of phase-locked loops at IF. The loop extracts the carrier from the modulated signal emitted by the caller and this is sent to each remote antenna which also

has its own loop. The differential phase is measured at the individual stations, quantized and sent back to the reference (base) station. The base station also extracts the modulation bearing the caller's address code. This information is sent via a downlink to the ground terminal where the data are recovered and processed by a resident computer.

It has therefore been concluded that the second system design is completely feasible from the electrical system point of view.

Finally a third system concept, called the Simultaneous Transform Array, was developed. The new array system operates in a manner analogous to an optical lens. The array elements phase-shift an impinging target wavefront so as to focus it on an energy-detecting image surface. The entire target image will be recovered from the image surface rather than through the point-by-point manipulation of array element outputs. This system was not developed analytically because it was beyond the scope of the present effort. Although the second system concept has been found satisfactory, it is felt that this new concept should also be considered as an alternative design if needed.

In Task 2, an experiment was conducted with the primary intention of obtaining some measured estimate of the maximum size of a ground based antenna array which could simulate a spaceborne system under different atmospheric conditions. The maximum baseline in the experiment was 800 feet. It was found that the RMS fluctuations in the phase difference for all measurements (of signals transmitted by the ATS-6 satellite) as a function of spacing between receivers was no more than 1° . Hence it was concluded that an earthbound experiment with an aperture of 800 feet would be indistinguishable from one in space.

Thus in Section 2 the various system concepts are developed and their respective performances analyzed. In Section 3 the results of the experiment are analyzed. In Section 4 it is concluded that system concept two is completely feasible from the electrical point of view, and it satisfies all of the system requirements. Further the experimental part of the project was satisfactorily completed. Finally, in Section 5 recommendations for further work are detailed.

2. ARRAY-IN-SPACE SYSTEM CONCEPT DEVELOPMENT

2.1 GENERAL OBJECTIVES

The main object is to design a large spaceborne array with many elements randomly located in a near-planar surface, for the formation of high angular resolution beams. The purposes of the array may include:

- a. The location of a disabled air or surface vehicle in distress by direction finding on an emergency microwave emission from the vehicle.
- b. Multiple-frequency high angular resolution beam-forming for communicating with multiple ground sources and/or monitoring sources of radio interference.

In general we confine our attention to a spaceborne receiving array, thus avoiding the severe microwave power generation and distribution problems that would result if the array were required to transmit rather than, or as well as, receive. While a geostationary orbit satellite is conceptually attractive, lower orbit cases may also be considered, since the extreme distance of the geostationary orbit may be prohibitive for some applications.

In line with the general objectives discussed above, it is possible to postulate a list of system characteristics that would appear to be necessary.

1. To achieve beam formation from a spaceborne array giving resolution of about 1 km on the ground would require an array size of H wavelengths where H is the satellite height in km. Thus at L-band, a geosynchronous satellite array would have to be 7 or 8 km in diameter to provide the indicated resolution θ ($\approx 60\lambda/D$ degrees, when D is the array diameter).
2. Radio Camera operation is possible since fixed or floating reference sources can be provided on the earth's surface for synchronization of the spaceborne array as well as for calibration of its pointing directions. It should be easier to locate the position of an unknown earth-bound source with respect to a nearby (set of) reference source(s) than if absolute accuracy were required.
3. Array elements can have "reasonable" gain since only the visible earth surface need be illuminated. Reference sources can be made strong enough (ground-based power and directivity) to insure high SNR at each element to permit accurate beam formation. Subsequent scanning of high resolution beams (in both space and frequency) then can permit adequate detection and hence location of unknown sources.
4. Assuming 2000 elements located at random over an 8 km circle, the average spacing between elements will be on the order of 150-200 meters. Signal flow problems must be solved for RF, local oscillator, IF, video and power supply as well as position stabilization/calibration

of element structures. To collect data at a central point in the array will require delays up to $4 \times 10^3 / 3 \times 10^8$ or 13.3 microseconds. The ability to achieve coherent spatially correlated beam formation would thus apparently impose the requirement that signal bandwidth be limited to no more than a few tens of kilohertz unless delay-lines were included in the design.

5. It will be important to quantify how accurately it will be possible to determine element location. This will serve to limit the extent to which beam scanning can be performed and hence will determine required spacing of reference sources (in both position and frequency).
6. L-band is probably a desirable design objective; lower frequencies would require greater size of array for comparable resolution while higher frequencies may make the system more vulnerable to weather and atmospheric anomalies although the smaller antenna sizes required make this an alternative worth considering.
7. The geosynchronous orbit assumed in the above discussion provides continual satellite presence and simplifies satellite location from the ground. However, a lower satellite orbit can provide orders of magnitude more SNR for received signals as well as requiring much smaller antenna size for equivalent resolution/accuracy on the ground.

It is apparent from the above list that while the concept shows promise, each item immediately suggests a host of questions that must be answered.

2.2 FIRST SYSTEM CONCEPT: Self-Cohering Radio Camera^{*}

The aim is to develop a system for accurate determination of the positions and the frequencies of the radiating sources which are located on (or close to) the earth's surface and whose radiation frequencies range between some minimum frequency f_{\min} and some maximum frequency f_{\max} . The idea is to employ a large random receive array in a geostationary orbit; spectral analysis of the received signals and beam formation after that will give the frequencies of the radiating sources as well as their angular locations within the array coordinate system; the longitudes and the latitudes of the radiating sources then can be easily found by relating the angular positions of the points on the earth's surface in the earth's coordinate system to the angular locations of the source points in the array coordinate system. (See Appendix I)

Our goal is to achieve accuracy in position determination on the order of one kilometer. This can be facilitated if the beams on the earth's surface are on the order of 1 kilometer wide. Taking into account that the distance between the geostationary orbit and the earth's surface is roughly 40,000 kilometers one finds that the required angular beamwidth would be

$$\gamma = 25 \times 10^{-6} \text{ radians.} \quad (2.1)$$

^{*}This system, although technically feasible, is discarded as impractical because of the nature of the earth-based beacon subsystem which it requires. The reader may choose to go directly to the second system concept found in Section 2.3 which does not have the same limitation.

This implies that we have to deal with an array of size equal to

$$D = \frac{\lambda}{\gamma} = 40,000 \lambda \quad (2.2)$$

Where λ is the wavelength of the received radiation.

Although in principle we can scan throughout the whole visible (from the array) part of the earth's surface, scanning in the neighborhood of the edges of the earth's disc would not be practical because (a) the angle between the line of sight and the earth's surface becomes too small to permit satisfactory accurate position location and (b) many of the radiating sources located in these regions will be screened out by mountains, forests and other obstacles. For these reasons, we will be concerned only with that part of the visible region for which the angle between the line of sight and the earth's surface is greater than 20° . The associated geometry is presented in Figure 2.1.

As seen, the maximum scanning angle $\theta_{1\text{max}}$ (measured from the line which connects the center of the earth with the location of the array) would equal 8.16° . Further, one can easily find (from $\theta_{1\text{max}} = 61.84^\circ$) that about 26% of the earth's surface would be inside the region of interest.

Determination of the positions of the microwave sources requires scanning in the (u-v)-plane on the earth's surface. Determination of the frequencies of the radiating sources will require scanning in frequency. If we generalize the meaning of the term "position" so that it includes a frequency coordinate besides the spatial coordinates, we can view the positions of any radiating source as a point in the u-v-f space. Figure 2.2

ORIGINAL PAGE IS
OF POOR QUALITY

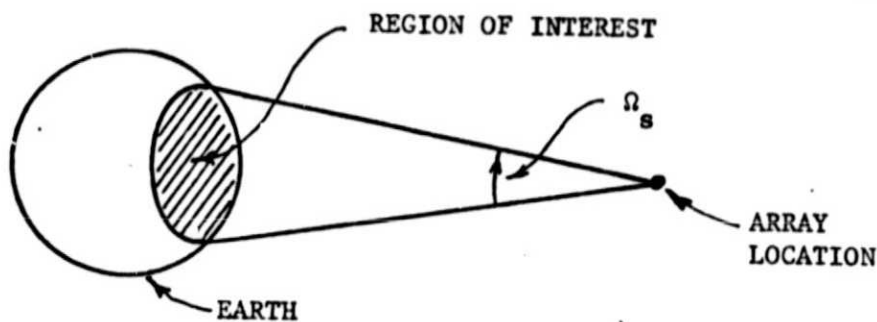
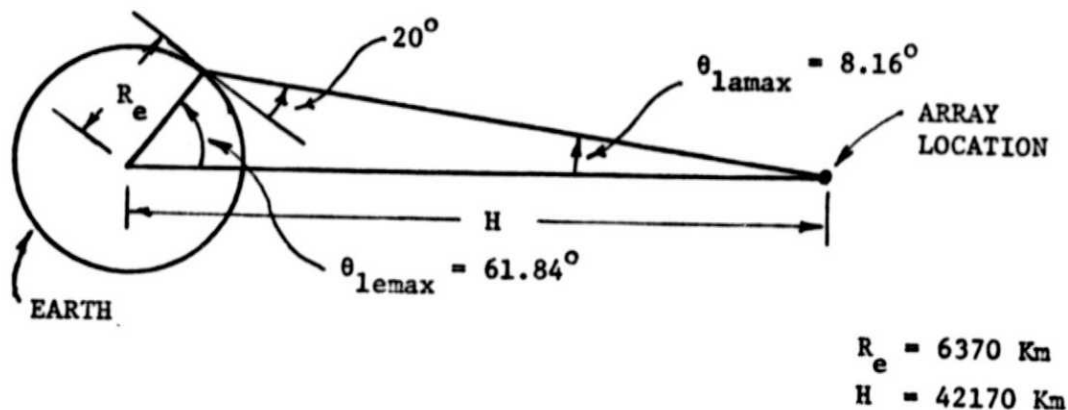


Figure 2.1 BASIC COVERAGE GEOMETRY

shows the shape of the volume within which the radiating sources of interest will be located and through which we will have to scan. In the figure u_o and v_o are angular coordinates of the earth's center. In the special case when the array is horizontal, these coordinates equal zero. f_{min} and f_{max} are the minimum and the maximum frequencies of interest, respectively.

The horizontal cross-section of the volume presented is roughly circular for small values of u_0 and v_0 (such as can be expected regarding our system) and is an exact circle when $u_0 = v_0 = 0$. The radius of this circle equals

$$r_b = \sin\theta_{l_{\max}} = 0.142 \quad (2.3)$$

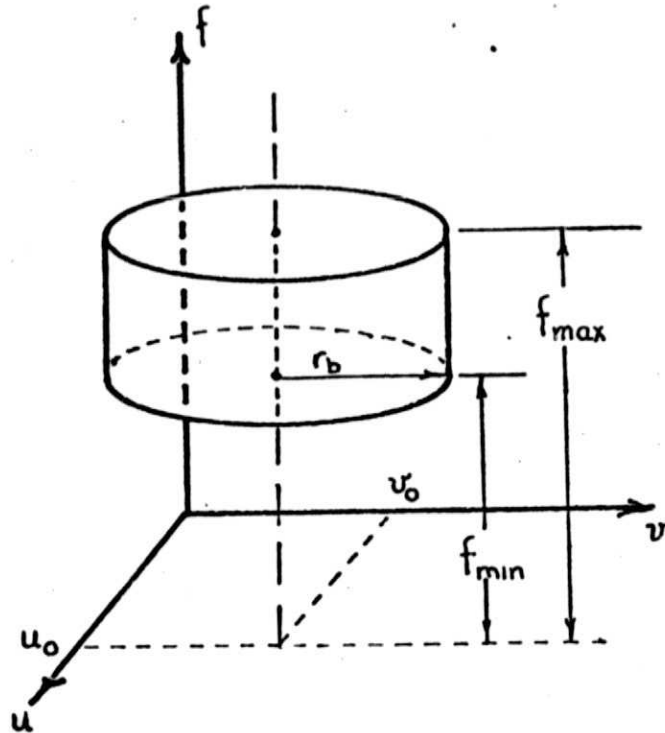


FIGURE 2.2 VOLUME OF SCANNING IN $u-v-f$ SPACE

At this point it is convenient to determine the number of angle-frequency resolution cells the system will have to deal with. Clearly this number will depend on the resolving power of the system in space and

frequency and on the dimensions of the volume in Figure 2.2. We have already made assumptions regarding the size of the angular resolution cells and the spatial dimensions of the volume. From them one can determine the required number of angular resolution cells. Thus, since the area of the 3 dB intersection of a beam in the u-v space approximately equals γ^2 and since the area of the horizontal intersection of the volume in Figure 2.2 is πr_b^2 , we find the number of angular resolution cells to be

$$L_e = \frac{\pi r_b^2}{\gamma^2} \doteq 1.013 \times 10^8 \quad (2.4)$$

To find the number of frequency resolution cells we must assume certain values for the difference $f_{\max} - f_{\min}$ and the required resolution in frequency, δ . Arbitrarily we choose 320 MHz for $(f_{\max} - f_{\min})$ and 100 KHz for δ and for these values we obtain the number of frequency resolution cells to be

$$L_f = \frac{f_{\max} - f_{\min}}{\delta} = 3200 \quad (2.5)$$

The values of $(f_{\max} - f_{\min})$ and δ can be in principle larger or smaller. However there is an upper bound on the value of δ above which we cannot go. Namely, if we are to achieve an angular accuracy approximately equal to the width of the beam, we cannot take for δ a value greater than the array bandwidth. (This is discussed in Appendix II).

Table 2.1 gives the array bandwidth values that correspond to a 40000 wavelength array for four different working frequencies and at three different scanning angles. (the angles are measured from the broadside direction). (See Appendix IV). For the system of concern the values in the left column can be considered as an upper limit of δ .

frequency	array size	array bandwidth [kHz]		
		$\theta_s = 2.5^\circ$	$\theta_s = 5^\circ$	$\theta_s = 10^\circ$
1 GHz	12 km	489	245	123
2 GHz	6 km	978	489	246
4 GHz	3 km	1956	979	491
8 GHz	1.5 km	3911	1958	983

TABLE 2.1 ARRAY BANDWIDTH

From (2.4) and (2.5) it follows that the total number of angle-frequency resolution cells is

$$L = L_e \times L_f = 3.242 \times 10^{11} \quad (2.5)$$

To interrogate a volume in the u - v - f space we synchronize the array by a reference source positioned at some point (u_o, v_o, f_o) , usually in the central region of the volume of interest, and then scan around that point. How far one can go from the synchronizing point (u_o, v_o, f_o) , or more precisely, what will be the shape and the size of the volume that can be covered by scanning, will depend on the uncertainties of the array element location. We have shown in Appendix III, that in the special case when the rms uncertainties of the array element location are equal along all the three axes of a rectangular coordinate system, i.e., $G_x = G_y = G_z$, the shifts in angle and frequency (Δu , Δv , and Δf) from the reference source must satisfy the inequality

$$\left(\frac{\Delta f}{f_o}\right)^2 + (\Delta u)^2 + (\Delta v)^2 \leq \left(\frac{c\sqrt{3}}{10f_o\sigma_r}\right)^2 \quad (2.7)$$

In the equation above f_0 is the frequency of the reference source, C is the speed of light and $\sigma_r = (\sigma_x^2 + \sigma_y^2 + \sigma_z^2)^{1/2}$ is the rms uncertainty of the array element location. It is easy to see that the volume within which one can scan is an ellipsoid centered around the reference source position. The dimensions of this ellipsoid are given in Figure 2.3. As can be seen, they are inversely proportional to the rms uncertainty σ_r . In the discussion to follow we will use the above mentioned special case as a model for analysis of our system.

For an array as large as 40000 wavelengths it seems reasonable to assume an rms uncertainty σ_r whose magnitude is of the order of 10 wavelengths.

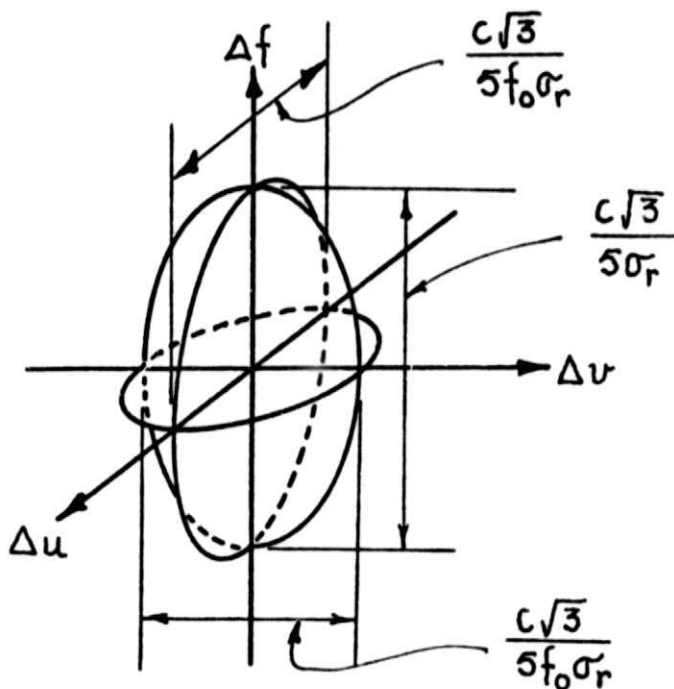


FIGURE 2.3 MAXIMUM SIZE OF SCANNED VOLUME

If we make such an assumption, then the dimensions of the ellipsoid in Figure 2.3 will be much smaller than the dimensions of the volume of interest in Figure 2.2. Therefore many reference sources will be needed to cover it. To determine the number of reference sources required, we will have to assume certain distribution of the reference sources throughout the volume of interest (Figure 2.2) and to find the required distances in frequency and space between the neighboring reference sources. For reasons of practicality we assume a distribution as the one given in Figure 2.4. Such a distribution can be obtained if we distribute on the earth surface multiple frequency transmitters in such a way that in the $u - v$ plane they form an approximately square lattice as shown in Figure 2.5.

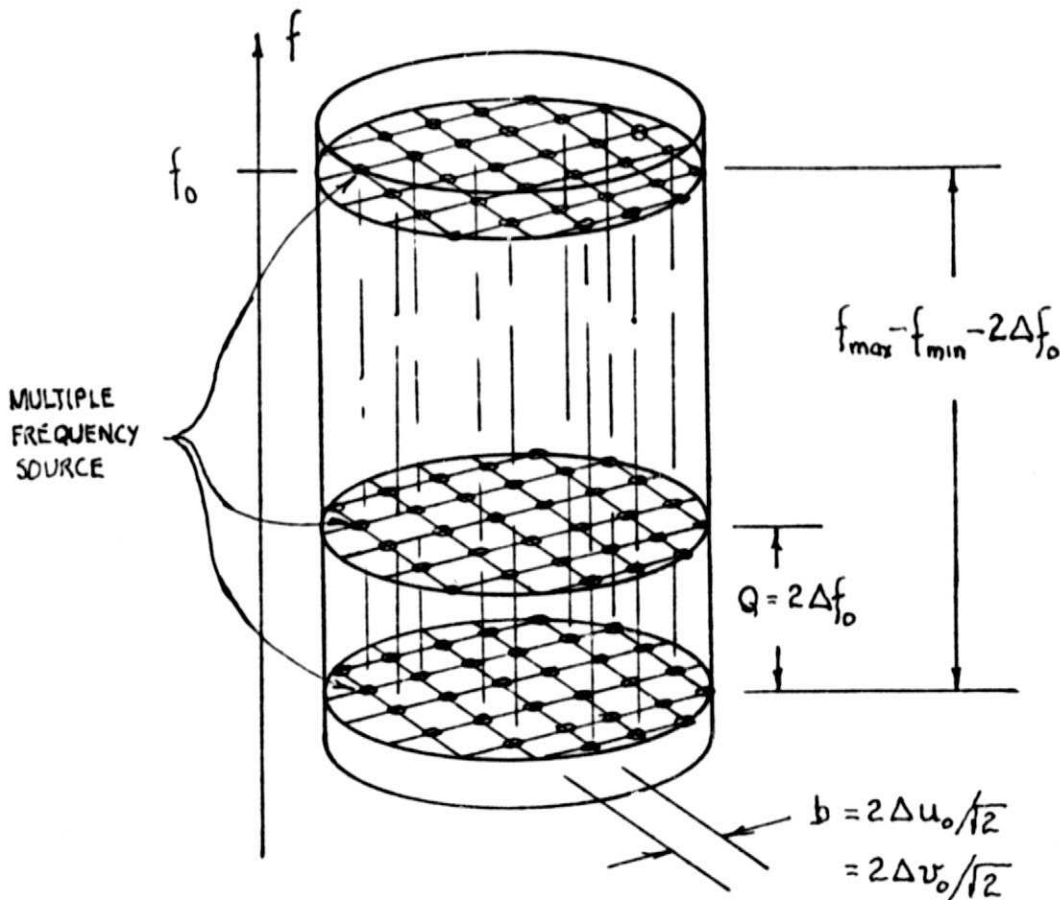


FIGURE 2.4 SOURCE DISTRIBUTION IN $u-v-f$ SPACE

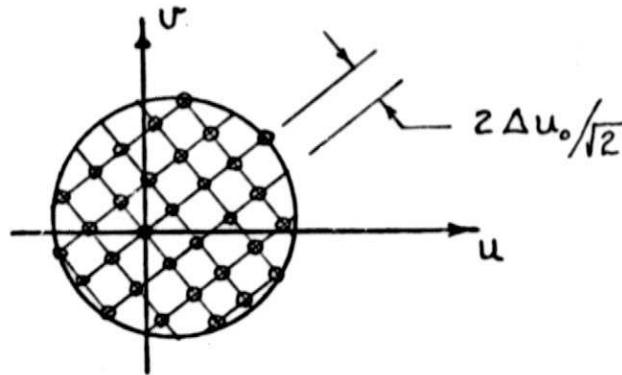


FIGURE 2.5 SOURCE DISTRIBUTION IN u-v PLANE

For the sake of simplicity in processing and to avoid unnecessary overlapping between the regions of two reference sources, instead of scanning throughout an ellipsoid we will associate with each reference source a scanning volume of the shape of a rectangular parallelepiped. This scanning volume will have orientation as that shown in Figure 2.6. Its dimensions $2\Delta u_0$, $2\Delta v_0$ and $2\Delta f_0$ will be chosen in such a way that they satisfy *

$$\frac{\Delta f_0}{f_0} = \Delta u_0 = \Delta v_0 \quad (2.8)$$

$$\left(\frac{\Delta f_0}{f_0}\right)^2 + (\Delta u_0)^2 + (\Delta v_0)^2 = \left(\frac{c\sqrt{3}}{10f_0\sigma_r}\right)^2 \quad (2.9)$$

*Note that this is the largest rectangular parallelepiped that can be circumscribed by the ellipsoid depicted by (2.7).

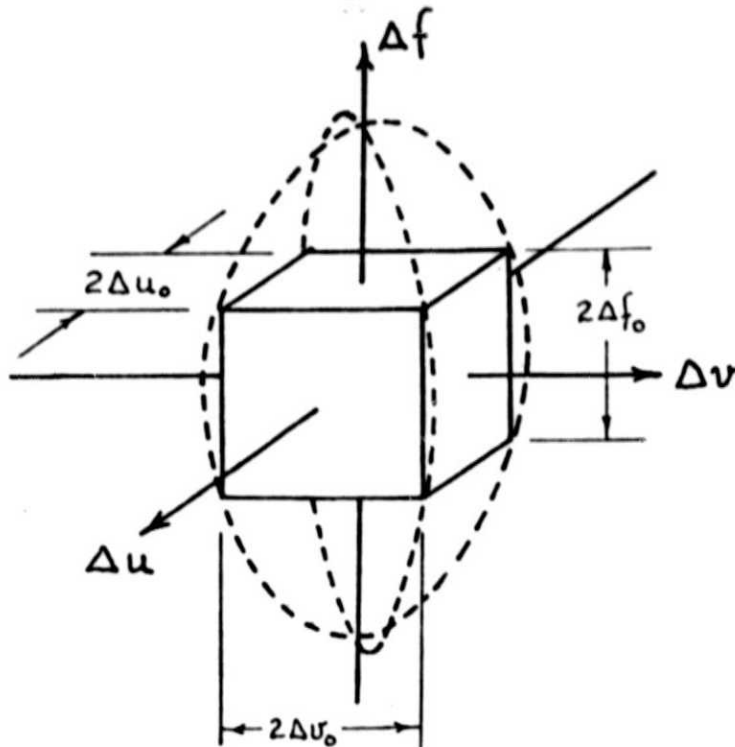


FIGURE 2.6 ACTUAL SCANNED VOLUME

Solving (2.8) and (2.9) one finds

$$\frac{\Delta f_o}{f_o} = \Delta u_o = \Delta v_o = \frac{C}{10f_o \sigma_r} \quad (2.10)$$

It is easy to see that in order to cover the volume of interest (Figure 2.2) by associating with each reference source (Figure 2.4) a scanning volume of the form, size and orientation given in Figure 2.6, the separations between the neighboring sources (Figure 2.4) will have to be

$$\text{along the frequency axis:} \quad a = 2\Delta f_o \quad (2.11)$$

$$\begin{aligned} \text{in the } u - v \text{ plane}^*: \quad b &= 2\Delta u_o / \sqrt{2} \\ &= 2\Delta v_o / \sqrt{2} \end{aligned} \quad (2.12)$$

* We take $b = 2\Delta u_o / \sqrt{2} = 2\Delta v_o / \sqrt{2}$ instead of taking $b = 2\Delta u_o = 2\Delta v_o$ since we want to keep the orientation of the scanning volume fixed for the $u - v$ plane, i.e., independent of the orientation of the lattice of transmitters in the same plane.

Combining (2.11) and (2.12), and using (2.10) yields

$$a = \frac{C}{5\sigma_r} \tag{2.13}$$

$$b = \frac{C}{5f_o\sigma_r\sqrt{2}} \tag{2.14}$$

In Table 2.2 we give the values of a and b for several values of f_o , assuming

$$\sigma_r = 20\lambda_o = 20C/f_o$$

$\sigma_r = 20\lambda_o = 20C/f_o$; R = 37000 km			
f_o [GHz]	a	b	b x R
2	20 MHz	± 0.007	261 km
4	40 MHz	± 0.007	261 km
8	80 MHz	± 0.007	261 km

TABLE 2.2 MAXIMUM SEPARATIONS IN SPACE (b) AND IN FREQUENCY (a) BETWEEN THE REFERENCE SOURCES.

From (2.14) we calculate the number of transmitters required

$$N_T = \frac{\pi r_b^2}{b^2} = \frac{50\pi r_b^2 \sigma_r^2 f_o^2}{C^2} \tag{2.15}$$

The number of discrete CW signals per transmitter follows from (2.13)

$$M = \frac{f_{\max} - f_{\min}}{a} = \frac{320 \times 10^6}{(C/5\sigma_r)} \tag{2.16}$$

Table 2.3 gives the values of N_T and M for several values of f_o , assuming $\sigma_r = 20\lambda_o$

$\sigma_r = 20\lambda_o = 20C/f_o$		
f_o [GHz]	N_T	M
2	1267	16
4	1267	8
8	1267	4

TABLE 2.3 NUMBER OF REFERENCE TRANSMITTERS (N_T) AND CW SIGNALS PER TRANSMITTER (M) REQUIRED.

NOTE:

Since the spatial separation between the reference sources is taken to be by $\sqrt{2}$ smaller than the spatial dimensions of the scanning volume (rectangular parallelepiped), there will be overlapping between the scanning regions associated with two neighboring reference transmitters. Therefore the actual number of angle-frequency resolution cells to be interrogated will be by a factor of 2 larger than the value given in (2.6). Thus we have

$$L = 6.482 \times 10^{11} \text{ (angle-frequency resolution cells)}$$

In conclusion, the system analysed above has the following disadvantages:

- (i) The high beacon density imposes a requirement that must be distributed uniformly anywhere on the earth's surface. This is impractical since beacons cannot be located on the oceans and they can only be located in countries willing to cooperate.

(ii) A large number of computations must be made for the large number of cells (in the u-v-f space) that must be searched.

(iii) The large number of beacons, and the requirement that each beacon has to transmit at a number of frequencies (Table 2.3), imposes a major installation and maintenance problem.

For these reasons it was decided that this system concept should be abandoned for the more feasible design of system concept 2, which is described next.

2.3 SECOND-SYSTEM CONCEPT: Self-Surveying Radio Camera

The system analyzed above imposes an unacceptably small spacing between beacons. It is not the large number of beacons per se that represents the problem, for the amount of equipment required for constructing and maintaining these beacons is miniscule compared to the spaceborne part of the system. Instead the uniformly high beacon density imposes a requirement that beacons may be placed arbitrarily anywhere on the earth. Beacons can not be so deployed, however. They can not be conveniently located on the oceans and they can only be located in those countries willing to cooperate. Thus the high beacon density is an intrinsic limitation.

Another factor which makes the high beacon density system questionable is the suspicion that with so large a number of beacons on the earth it should be possible to dynamically survey the element positions of the spaceborne array and thereby preclude the necessity for self cohering.

With these factors in mind an alternate system concept was developed. The concept is based on the assumption that an element location substation can be created consisting of beacons clustered on the land masses and distributed over the small angle subtended at the geosynchronous satellite by the earth.

Given that assumption it is only necessary that each array module in the spaceborne system be able to measure the phase, or at most the amplitude and phase, of the radiation field at sufficiently frequent time intervals and transmit this information to the earth. The complex samples and the locations from which the samples were taken, constitute the only information required by a signal processor to locate the angular coordinates of the source or sources.

Thus in Section (2.3.1) the problem of surveying the elements of the array is discussed. In Section (2.3.2) a position finding algorithm, for locating the transmitting sources, is introduced, which has many common features with the surveying algorithm of Section (2.3.1). In Section (2.3.3) the required electronic system is discussed.

2.3.1 ARRAY ELEMENTS SURVEY

As a consequence of the study of the second system concept, it was found imperative that the positions of the elements of the randomly distributed spaceborne antenna array should be surveyed [1]. Thus given a set of transmitting beacons on the earth's surface, the objective is to locate the position of the elements of the array using a set of phase measurements of the originals transmitted by the beacons together with the knowledge of the transmitting frequencies and the positions of the beacons. The algorithm of solution is based on the use of phase measurements at the antenna elements of signals transmitted by a set of well determined randomly distributed sources (beacons) on the earth's surface. The results so derived are unique for the given set of measurements. The algorithm is essentially based on the method developed in [2], (see Appendix V), for surveying

an array in the far field. In this section, we will simply sketch the outline of the algorithm and briefly state the results for the spaceborne array. A full description of the algorithm and the main results may be found in Appendix V.

Consider a set of N receiving elements which make up the spaceborne antenna array. Let $\underline{r}_i = (x_i, y_i, z_i)^T$ be the vector of unknown rectangular coordinates of the i th element, with respect to a reference element at the origin. Assume that for sinusoidal excitations induced in the elements, the phase at each element relative to reference element at the origin can be measured. The objective is to compute \underline{r}_i .

Suppose a beacon (on the earth's surface) B_j , with known coordinates, radiates energy at wavelength λ , arriving at the array of elements as a plane wave at elevation $(90 - \theta_j)^\circ$ and azimuth ϕ_j . We will characterize such a beacon by its wave vector

$$\begin{aligned} \underline{k}_j &= \frac{2\pi}{\lambda} (\sin \theta_j \cos \phi_j, \sin \theta_j \sin \phi_j, \cos \theta_j) \\ &= \frac{2\pi}{\lambda} (a_j, b_j, c_j) \end{aligned} \quad (2.17)$$

where $a_j = \sin \theta_j \cos \phi_j$, $b_j = \sin \theta_j \sin \phi_j$, and $c_j = \cos \theta_j$. The absolute phase at the i th-element of the array, relative to a reference element, ψ_{ij} , due to a signal from B_j is given by

$$\psi_{ij} = \frac{2\pi}{\lambda} (a_j x_i + b_j y_i + c_j z_i) \quad (2.18)$$

The measured phase is in fact $\tilde{\psi}_{ij} = (\psi_{ij}) \pmod{2\pi}$, i.e.

$$\tilde{\psi}_{ij} = \frac{2\pi}{\lambda} (a_j x_i + b_j y_i + c_j z_i) + 2\pi n_{ij} \quad (2.19)$$

$$j = 1, 2, \dots, M$$

where n_{ij} is some integer, and M is the number of beacons. Equation (2.19) is repeated for each element of the array, $i = 1, 2, \dots, N$. For the i th-element, (2.19) may be rewritten in matrix form as

$$\frac{1}{2\pi} \begin{bmatrix} \tilde{\psi}_{i1} \\ \tilde{\psi}_{i2} \\ \vdots \\ \tilde{\psi}_{iM} \end{bmatrix} = \frac{1}{\lambda} \begin{bmatrix} a_1 & b_1 & c_1 \\ a_2 & b_2 & c_2 \\ \cdot & \cdot & \cdot \\ a_M & b_M & c_M \end{bmatrix} \begin{bmatrix} x_i \\ y_i \\ z_i \end{bmatrix} + \begin{bmatrix} n_{i1} \\ n_{i2} \\ \vdots \\ n_{iM} \end{bmatrix} \quad (2.20)$$

for $M \geq 4$, and assuming the beacons are randomly distributed, it is easy to show that the solution vector \underline{r}_i of (2.20) is essentially unique [2]. This result may then be used to determine, from the vector of observed phases $\tilde{\psi}_i$, the i th-element position vector \underline{r}_i .

In general, the relative phase vector measured at the array is $\hat{\psi}_i = [\hat{\psi}_{i1}, \hat{\psi}_{i2}, \dots, \hat{\psi}_{iM}]^T$ and not $\tilde{\psi}_i$, where $\hat{\psi}_i$ is $\tilde{\psi}_i$ corrupted by random phase errors. A least squares fit $\hat{\underline{r}}_i$ to the observed phase vector $\hat{\psi}_i$ therefore provides one estimate of \underline{r}_i . For this purpose, an error function $F(\underline{r}_i)$ is defined as follows:

$$F(\underline{r}_i) = \sum_{j=1}^M \{ [\tilde{\psi}_{ij}(\underline{r}_i) - \hat{\psi}_{ij}] \pmod{2\pi} \}^2 \quad (2.21)$$

where $(x) \pmod{2\pi} \hat{=} x + 2\pi n$ for some integer n such that $-\pi < x + 2\pi n < \pi$, with $\tilde{\psi}_{ij}(\underline{r}_i)$ being the relative phase shift (modulo 2π) generated at the i th element by the j th beacon. We are looking for a position vector $\hat{\underline{r}}_i$ minimizing the error function; clearly, in the noise free case when $\tilde{\psi}_i = \hat{\psi}_i$, we have $\hat{\underline{r}}_i = \underline{r}_i^* \hat{=} \underline{r}_i$ the true position vector.

Considering the overall characteristics of this error function, initially assuming the noise free situation, when \underline{r}_i is not in the vicinity of \underline{r}_i^* , the quantity under the summation in (2.21) acts as the square of a random variable uniformly distributed over $(-\pi, \pi)$. Thus the average value \bar{F} of the error

function in this case is given by

$$\bar{F} = \frac{M\pi^2}{3} \quad (2.22)$$

when r_i is close to r_i^* we can obtain a first order approximation to $F(r_i)$ by using a Taylor series expansion around $r_i = r_i^*$. This yields the expected value $E\{F(\Delta r_i)\}$, given by

$$E\{F(\Delta r_i)\} = 4\pi^2 \left(\sum 1/\lambda_j^2\right) [F\Delta x_1^2 + F\Delta y_1^2 + G\Delta z_1^2] \quad (2.23)$$

where F and G are given by

$$F = \frac{1}{2} \left[1 - \frac{1}{3} (1 + \cos \alpha_u + \cos^2 \alpha_u) \right] \quad (2.24)$$

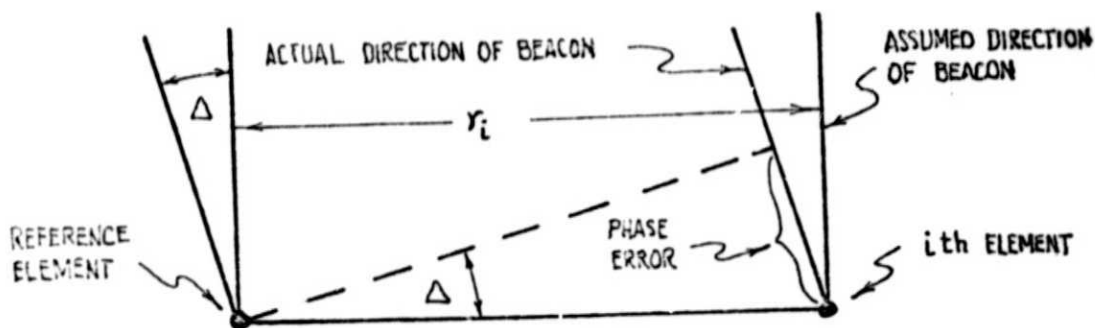
$$G = \frac{1}{3} [1 + \cos \alpha_u + \cos^2 \alpha_u] \quad (2.25)$$

This analysis of the error function is for the specific case when the sources are uniformly distributed over an area whose boundary subtends an angle $2\alpha_u$ about the z-axis. For the array in synchronous orbit, the angle of view is only 17° and hence $\alpha_u = 8.5^\circ$.

Using the above function, the uncertainty in element location was found to be of the order of $1/3\lambda$ in the x-y direction and 0.1λ in the z direction, assuming phase errors of $\pm 20^\circ$ [2].

The tolerance on beacon position may be computed as follows. Consider the following figure, which represents the worst case, when the *i*th element and the reference element are perpendicular to the direction of the signal from the beacon. We will assume that errors in measurement of phase due to noise and uncertainty regarding beacon position are within the range of $\pm 20^\circ$ (a figure which is easily attained with present day technology). From the figure on the next page it is easy to see that the phase error $\delta\psi_{ij}$ due to change in position of the beacon is given by

$$\delta\psi_{ij} = \frac{2\pi(r_i \Delta)}{\lambda} \underset{\text{assuming no noise} = \frac{\pi}{9}}{\leq \text{tolerance on phase measurement}} \Rightarrow \Delta \leq \frac{\lambda}{18r_i}$$



Assuming $r_i = 1$ km and $\lambda = 50$ cm, then $\Delta \leq 0.28 \times 10^{-4}$ rad. In other words if the antenna array is in geostationary orbit, at 40,000 km from the earth's surface, assuming $\lambda = 50$ cm, $r_i = 1$ km and phase tolerance of $\frac{\pi}{9}$, then the tolerance on beacon position ≈ 1.1 km which is very easy to achieve.

The tolerance on the frequency of the transmitted signal may also be computed [2]. Assuming a transmission frequency of 1 GHz, the tolerance on the frequency is ± 4 MHz. This implies that the beacons do not have to have very tight specifications.

The algorithm used for computing the position of the elements of the array is based on using a number of beacons which are near the center of the field of view (i.e., small aperture) to obtain a coarse grid on which to search for the element position. This is then followed by a finer grid formed by adding a number of beacons at the edges of the field of view (i.e., large aperture). For this purpose, a study was made to locate the set of beacons for different areas of search. Thus:

- (i) To cover the Atlantic: beacons are placed in Western Europe and the East Coast of U.S.
- (ii) To cover the South Pacific: beacons on the West Coast of U.S., Hawaii and Australia.
- (iii) to cover the Indian Ocean: Australia, islands in the Indian Ocean and South Africa.

2.3.2 SOURCE POSITION LOCATION ALGORITHM

The objective of the proposed space system is to estimate the angular coordinates of a radiating source on earth, based only on phase measurements. In this section we examine two different approaches that have been proposed and suggests a hybrid that possesses the advantages of both approaches. The desired accuracy is 25 μ rad corresponding to an error on the earth of 1km.

A. Interferometry

This is a classical technique that has been used in radio astronomy. Its use for azimuth angle estimation has been studied in a VFRC report [3] from which some analysis is borrowed. The method basically uses a series of antenna baselines of different lengths, in which the final angular accuracy is determined by the largest baseline and a shorter baseline is used to resolve the angular ambiguity in the next larger one. Some details are given in [4]. If the largest baseline is D_N we need $\delta D_N \approx 10^{-3} D_N$ where δD_N is $\approx 5\lambda$.

This accuracy may be achieved if the antenna baseline is almost rigid. With a moving baseline, however, such an accuracy is doubtful. Nevertheless it has the advantage of computing estimates in a shorter time period than the second method to be described now.

B. Angular location by Least Square Fit Method, (LSE)

This approach was reported in [5] and uses phase measurements from a random array. It is a brute-force method that involves scanning over the whole region of interest in the angular space to get minimum square error. Although the earth is within a 17° cone, the azimuth ϕ could be anywhere within $(0, 2\pi)$ and a search is too time consuming for the desired angular accuracy. However, the tolerances on element positions are more relaxed than for an interferometer, the working of which as mentioned above hinges on the accuracy of the largest baseline.

C. Proposed Method

Both methods A and B are attractive in complementary ways and it seems logical to consider a combination. We shall use two short, almost perpendicular, semi-rigid booms for interferometer baselines as shown in Figure 2.7. The rest of the array system will be discussed after examining the interferometer. The zeroth (reference) element is situated on the satellite itself. The objective is to use the interferometer to give quick, rough angle estimates without facing the tolerance problem alluded to earlier, then switch over to the LSE method which uses the rough estimates as initial values to achieve the final estimates that meet the accuracy requirements.

In this method, we make the following first-order assumptions:

- 1) the satellite coordinates relative to earth are known
- 2) the incoming wavefront is planar
- 3) there is no multipath interference
- 4) negligible propagation/refractive effects along its path
- 5) the elements do not move significantly during the phase measurements.

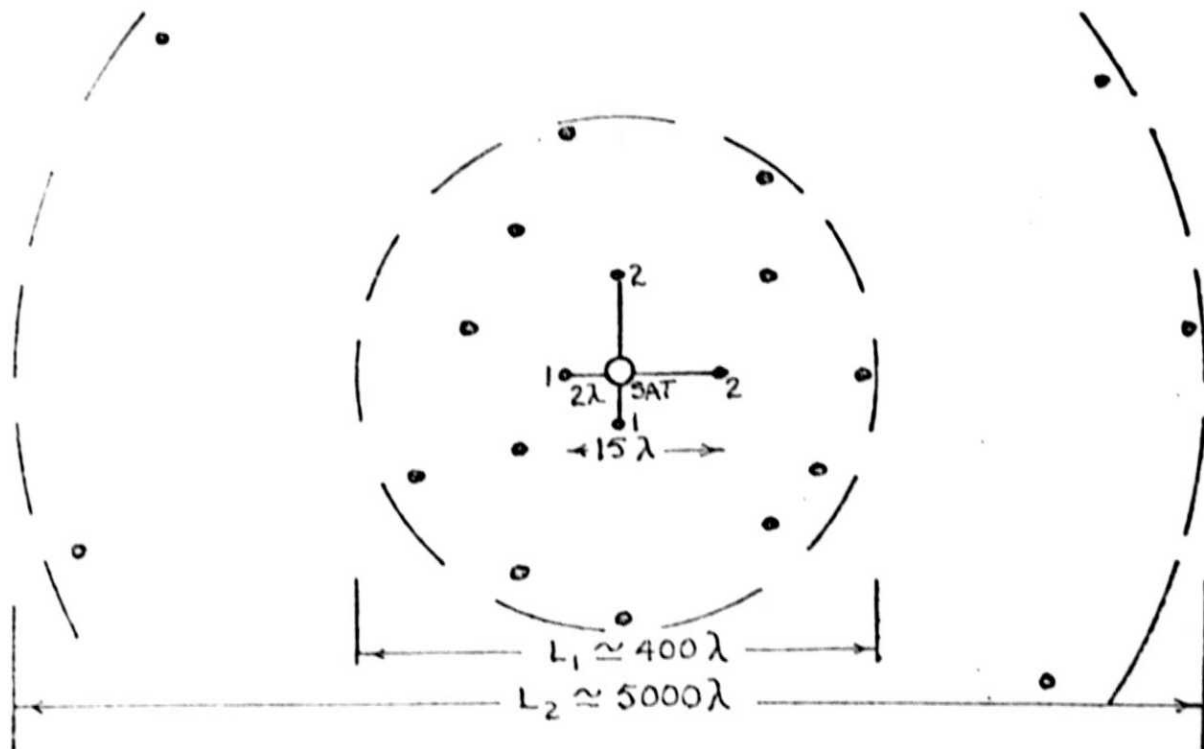


FIGURE 2.7 SATELLITE ANTENNA SYSTEM

Using the Interferometer

It is shown in [4] that the coarse accuracy of 3-5 milliradians can be achieved with 2 baselines per interferometer with $D_1 = 2\lambda$, $D_2 = 10\lambda$ to 15λ . In the space environment and with baselines of these magnitudes, it is assumed that variations due to temperature, gravity, etc. are negligible. The procedure for determining the source angles θ_T , ϕ_T in the satellite coordinates in Figure 2.8 are shown in [4]. These values are used as initial guesses for the next step, as follows.

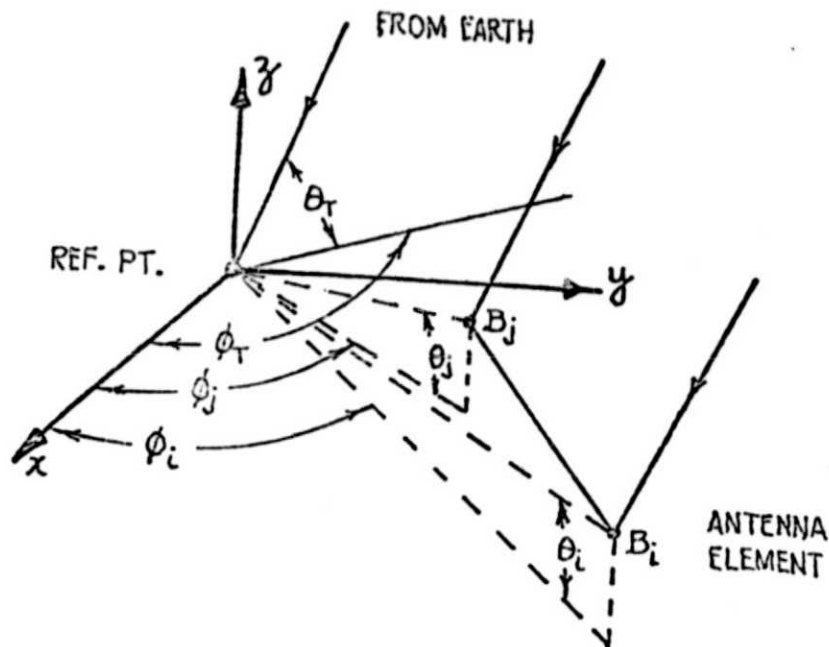


FIGURE 2.8 ANGLE RELATIONSHIP BETWEEN ANTENNA ELEMENT AND SOURCE DIRECTION.

Using the LSE Method

The final accuracy in angle estimation is determined by the extent L of the array. The accuracy can be viewed in the context of pointing errors in an array since, in that situation, the phase shifters are adjusted to point a beam in a certain direction while in the situation here the phases induced by a source in a certain direction are being measured. Thus we assume that for both elevation θ and azimuth ϕ

$$\sigma_{\theta}, \sigma_{\phi} \sim \sigma_{\phi} \left(\frac{\lambda}{L}\right) \frac{1}{\sqrt{N}} \text{ rad} \quad (2.26)$$

where σ_ϕ is the standard deviation of phase measurement error, λ/L is the nominal array beamwidth and N is the number of elements in the array (the error in azimuth could be an order of magnitude higher if the elevation angle θ_T is close to $\frac{\pi}{2}$ because of an additional term $1/\cos\theta_T$ for σ_ϕ).

The number of elements N is to be large enough to suppress the 'side-lobes' in the error function described in [5] and for more accuracy. A probabilistic approach is attempted in [4] to determine the number needed. We then need to determine how the elements are to be distributed. This is done as follows:

Given that the original uncertainty from the interferometer is 3 mr, let the next order of accuracy to be achieved be 0.3^2 mr. From (8), with $N_1 = 15$,

$$L_1 = \frac{\lambda \sigma_\phi}{3 \times 10^{-4} \sqrt{15}}$$

Also assume $\sigma_\phi^2 = \sigma_{\phi,t}^2 + \sigma_{\phi,q}^2 + \sigma_{\phi,el}^2 = 0.5 \text{ (rad)}^2$, where $\sigma_{\phi,t}$ (thermal noise) = 0.18 rad with SNR = 15db, $\sigma_{\phi,q}$ (quantization) = 0.06 rad with 5 bits representation; and $\sigma_{\phi,el}$ (element position) = 0.45 rad, corresponding to an error of about $\frac{\lambda}{10}$. Then, $L_1 = 400\lambda$. The algorithm begins with the interferometer estimates θ_0, ϕ_0 and searches over the region $\theta_0 \pm 0.003, \phi_0 \pm 0.003$ rad in steps of 0.3 mr, requiring 400 steps to get estimates θ_1, ϕ_1 .

Let the final uncertainty required be $25\mu\text{rad}$ and let $N_2 = 20$ elements. Then $L_2 = 5000\lambda$. This iteration requires $\left(\frac{0.0006}{25 \times 10^{-6}}\right)_6 = 576$ steps. The two iterations take a total of about 1000 steps for evaluating $F(\theta, \phi)$, the error function in [5].

The antenna element distribution is illustrated in Figure 2.7. If possible it is constrained to lie almost in a circle rather than a sphere with the earth direction at its broadside.

2.3.3 ELECTRONIC SYSTEM CONSIDERATIONS

The survey and source estimation algorithms have been discussed in Sections 2.3.1 and 2.3.2. As is shown later the computational requirements are excessive. The survey itself takes M seconds (assuming 1 sec per beacon frequency and M beacons) just to gather all the phase information and the elements would drift slowly even within this period.

The algorithm calls for an updated survey on detecting an emission on earth. The satellite then switches back to that particular caller frequency band to collect the necessary phase information to calculate the caller's angular position. This is immediately followed by a second survey. It is hoped that the element locations can be approximated by an 'interpolation' of the two survey results (which themselves are not very accurate owing to the element drifts).

All the information is sent down to earth and is stored on arrival in the computer. Note that the reference coordinates and the transformation parameters from satellite to earth coordinates at the appropriate times have to be known. Admittedly this is a weak link in the design because not only must these be accurately known but those values at an earlier time are required owing to propagation delays both in the satellite electronics and the transmission path of 40000 km.

Given that the above-mentioned information can be obtained, all the data processing need not be done in real time.

Sources

The sources on the earth are of low power, with low antenna gain, operating in the L-band. The power-gain product is of the order of 10 watts, at most 100 watts. Low power is assumed. The transmitter will be a small equipment easily handled and not requiring high performance. Low antenna gain is assumed so that care need not be taken by the user in orienting the antenna. The radiating frequency is controlled by a low cost crystal driving a frequency multiplier which results in one of N allowed frequencies occupying a band of width W Hz. Each transmitter will have a simple means to impart a simple address code or "call letters" of the user. One such possibility is a series of toggle switches or buttons. A 20-bit code would permit 10^6 addresses or separate users. Simple ON-OFF keying or binary phase shift keying would be adequate.

Information provided by Dr. Sajjad Durrani of NASA indicates that 15 MHz at each end of the 20 cm wavelength satellite band is relatively free at the

present time for such use. In the design discussed below, therefore, the value taken for W is 30 MHz.

Functional Block Diagram

Figure 2.9a is a block diagram of the system. The right-hand section is the reference element; the left-hand section is the array element. The signal from the source is radiated at frequency f_s . The front ends of both equipments are the same. Each has an antenna of conventional design, such as a dish or a horn. The antenna diameter is 2 to 3 wavelengths such that its beamwidth covers the entire earth. The RF bandwidth is W . A mixer is driven by a scanning frequency synthesizer. The IF bandwidth $B=W/N$ is the spacing between the N allowed frequencies within the band W . B is determined by the long term stability of the transmitting sources. Assuming a low cost oscillator, a stability of 1 part in 10^5 is readily achievable. Permitting some margin for error, and assuming a wavelength of 20 centimeters, B is of the order of 10^5 Hz.

This value is taken to be the drift tolerance of the source transmitter. It is not the short term bandwidth of the transmission, however. Instead the sources are assumed to be stable for the order of 10^{-2} seconds corresponding to a line spectral-width of 100 Hz. This fact is utilized by following the IF amplifier in the reference module by a bank of narrow-band filters each of 100 Hz bandwidth. A bank of 1000 filters is required for this process, probably implemented digitally. Envelope detection and low pass filtering for 1 second follow. Following integration, threshold and decision logic determine whether or not a signal is present, extracts its call letters or address, measures the frequency of the source, possibly alters the search pattern of the frequency synthesizer, and delivers signal-frequency information to the frequency synthesizer so that

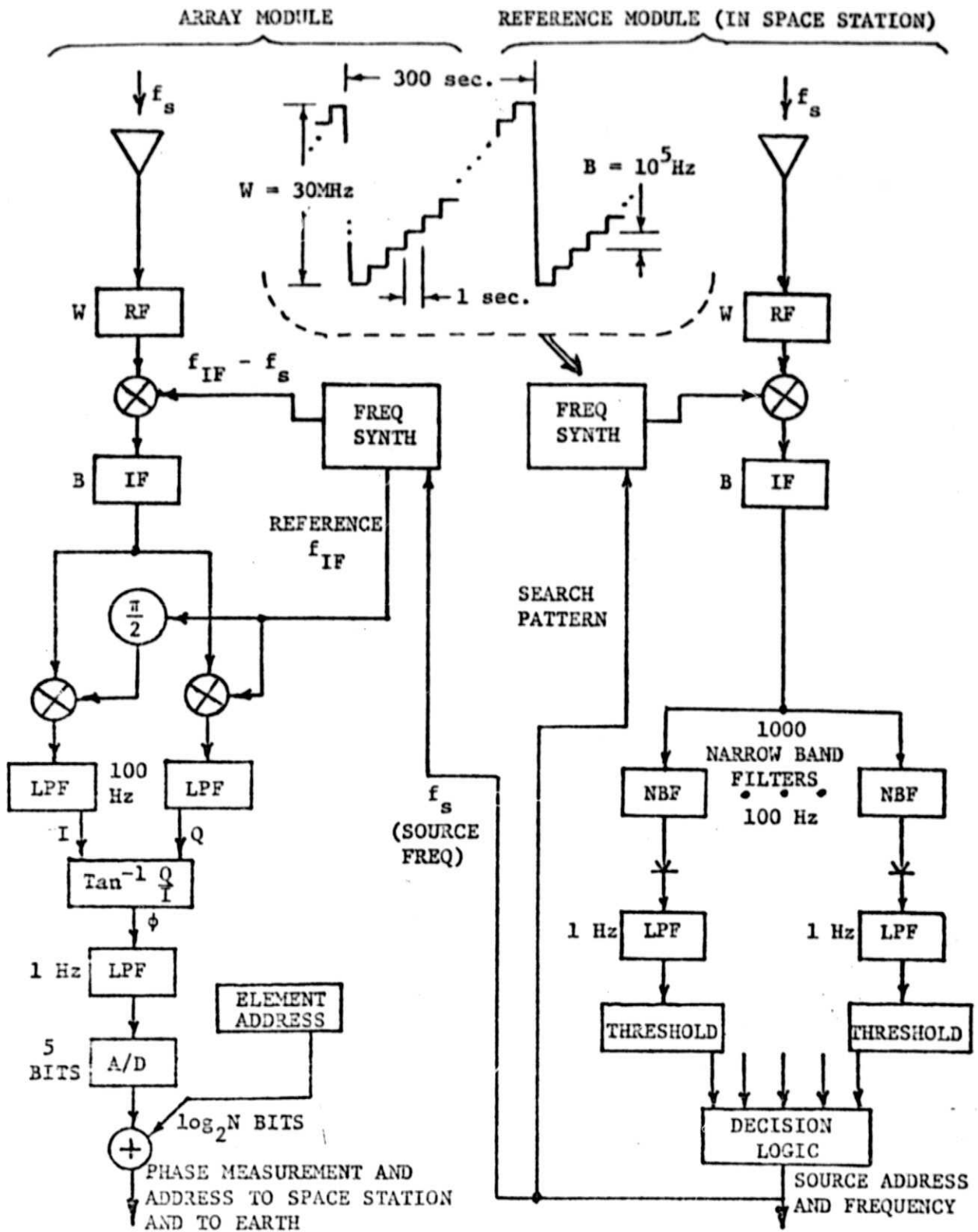


FIGURE 2.9a. BLOCK DIAGRAMS OF REFERENCE AND ARRAY MODULES.

the latter may provide the proper signals to the array element modules. In the lower part of the figure the received signal is heterodyned to the center of the IF passband where it is coherently quadrature demodulated. The signals of both channels are integrated in low pass filters of 100 Hz bandwidth. Amplitude and phase measurements can then be made. Only the latter is shown. The phase measurement is smoothed in a 1 second time constant low pass filter, after which the analog voltage is sampled and converted to digits. Five-bit precision is adequate. The element address is added to the five-bit word. The address requires $\log_2 N_e$ bits where N_e is the number of elements.

SNR Analysis

The signal-to-noise power ratio in the IF in the reference receiver and in each of the array element receivers is given by

$$r_{if} = \frac{P_T G_T A_R}{4\pi R^2 k T B F} \quad (36)$$

In (36) P_T is the transmit power source on earth, G_T is the source antenna gain, A_R is the area of the receiving antenna in each spaceborne module, R is the (geosynchronous) range (40,000 km), k is Boltzmann's constant, T is the effective temperature of the receiving systems, B is receiver bandwidth (10^5 Hz) and F is the noise figure. Since the receiving antennas are pointed toward the earth, a nominal earth temperature of 290° Kelvin is assumed, making $kT = 4 \times 10^{-21}$ watts/Hz. At L-band a noise figure of a few dB is available. To provide some margin $F = 10$ dB is assumed in this analysis. Assuming $P G_T = 10W$, $A_R = 4\lambda^2$ and $\lambda = 20$ cm, (36) evaluates to -17 dB. Coherent integration in the filter bank of the reference receiver and in the quadrature low pass filters of the array element receivers narrows the noise bandwidth to 100 Hz, thereby increasing the

signal-to-noise ratio by 30 dB to 13 dB. Noncoherent smoothing by a factor of 100 to 1 further increases the signal-to-noise ratio by nearly 20 dB. (The increase in signal-to-noise ratio through the post detection filter is approximately linear with the amount of integration because the input signal-to-noise ratio to the post detection filter is so much greater than unity.) The result is in excess of 30 dB.

The angle estimation is a function of the number of elements in the array which in turn will be influenced by the angle-measuring or direction-finding algorithm eventually chosen for the system; in general the larger the number of elements in the array the smaller is the SNR requirement per element. A conservative bound is obtained by considering the two element interferometer. The available angular accuracy is given by [26]

$$\Delta\theta \approx \frac{\lambda}{Lr^{1/2}} \tag{37}$$

In (37) L is the size of the interferometer base. The desired angular accuracy is the order of 1 km at a distance of 40,000 km, or 2.5×10^{-5} rad. Taking the signal-to-noise ratio to be 30 dB the maximum required array size is $L_{\max} = \frac{\lambda}{r\Delta\theta} = 1440$ m. A still more conservative estimate is obtained by assuming 30dB SNR as a margin for system and component troubles. For example a user in distress on the ocean cannot be expected to align the antenna correctly or even, perhaps, to ensure that it is not partially submerged. A 30dB margin would materially enhance that probability that the system works when it is needed. In this case the required array size becomes $L = \lambda/\Delta\theta = 8$ km.

Both numbers are large. An array compatible with this system concept will be measured in kilometers.

Satellite Electronics System

It is proposed that the earth-borne transmitters emit bursts of CW and BPSK signals alternatively, the latter containing a header for synchronization followed by the code letters. The CW is used for locking the loops as discussed shortly. BPSK is also used in the downlink to the earth station where data processing is to be done.

A more detailed system design is shown in Figure 2.9. The front end is modified as shown. The IF signal is fed into a Costas loop which conveniently provides both an unmodulated reference carrier $r(t)$ for phase comparison as well as the demodulated binary code $z(t)$ that identifies the caller. The loop must have a bandwidth large enough to track the center frequency of the BPSK input but small enough to avoid tracking the modulation itself. If the loop filter is chosen to have a cutoff at 50 Hz to accommodate the 100 Hz oscillator coherence bandwidth expected, then we require

ORIGINAL PAGE IS
OF POOR QUALITY

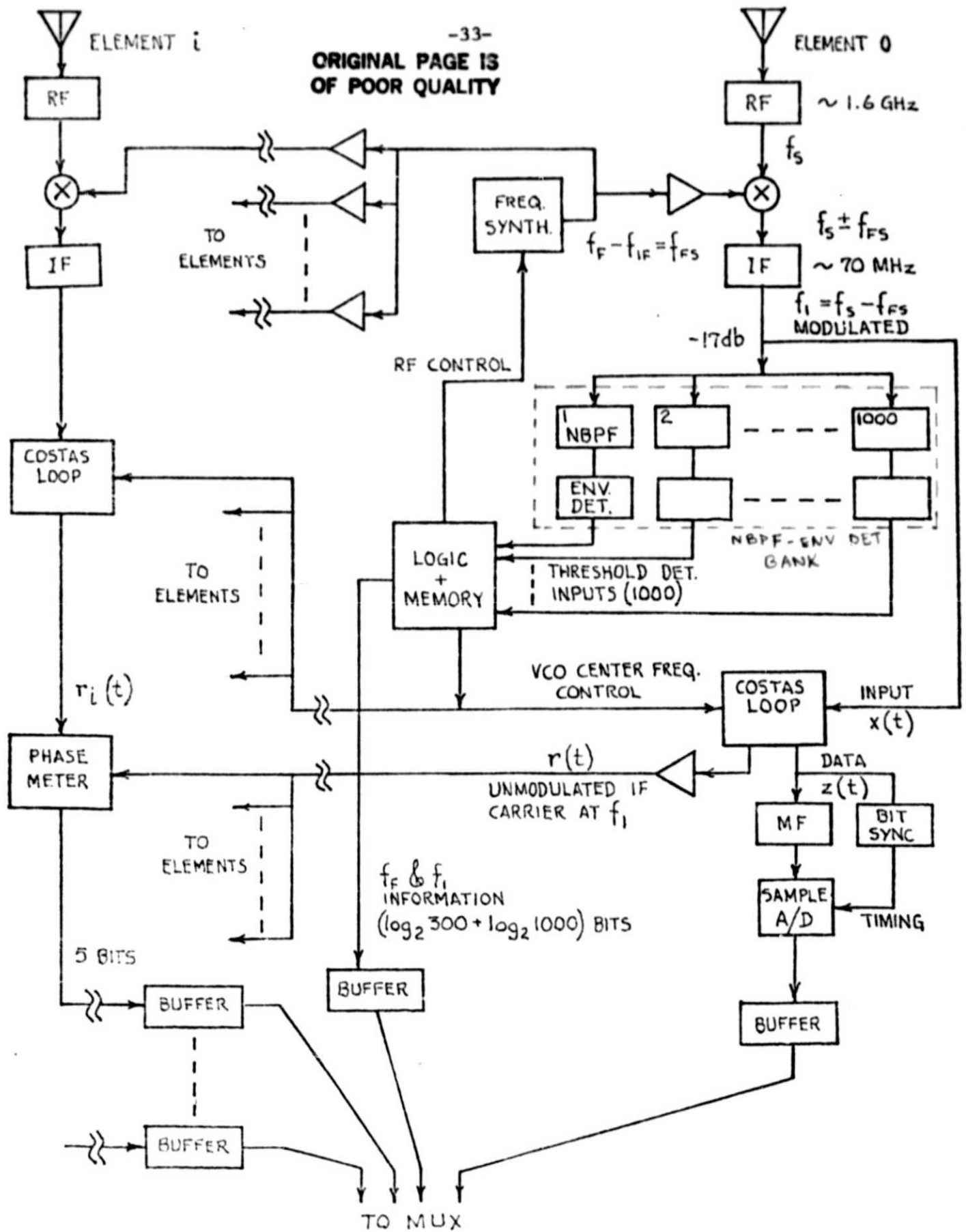


FIGURE 2.9 SATELLITE ELECTRONICS SYSTEM

the keying to exceed 50 Hz, say a 500 bps rate. (A conflict with the detection circuitry would arise if the input is continuous BPSK because the power is spread over several detectors in the bank. This is the reason for introducing short bursts of CW between the modulated waveform). The two LPF's in the Costas loop I-Q arms must be wide enough to pass the BPSK modulation, say 1.2 kHz. It is shown in the appendix in [6] that we require 500 bps rate BPSK transmitters operating at about 4 watts output.

The NBPF-envelope detector bank has 1000 channels and is designed to indicate in which band the center frequency lies. Assuming that the modulation is PN-like, then the PSK spectrum is of the $\sin x/x$ form with the main lobe within $f_1 \pm 500\text{Hz}$. Since the NBPF's have a bandwidth of 100Hz only, there would be little energy at their outputs even with a 1 sec signal duration. However, the output of one of the NBPF's would be large when the input is a CW burst and this would register a hit at the detection circuitry with the appropriate threshold.

On recognizing a hit in one of the 1000 channels, the logic stores this information as well as the RF band f_F and switches over to the survey frequency band for an update on the element locations and sends the phase and element address information via the data link. The only difference between surveying and listening to a caller is that the former is CW and no identification code is needed because each beacon has its own assigned frequency. The different procedures in handling both situations can be incorporated in the logic to save time, rather than including it in software.

On completion of the survey, the logic switches the RF local frequency back to f_F and sends a control signal that adjusts the free running frequency of the digital VCO in the Costas loop so that the IF signal at f_1 would be acquired. Once in lock, the loop provides the demodulated binary bit stream $z(t)$ for the source address and a coherent IF carrier $r(t)$ to be piped to the remote elements for phase comparison, bearing in mind that delays to every element must be equalized. Note that a filter matched to a bit in the code sequence $z(t)$ is used to maximize the SNR and hence reduce the bit error probability.

The other elements are separated from the reference station and, in addition to the IF signal, must be provided with (a) the RF local reference at f_{FS} and (b) the digital control signal from the base station logic that allows the

remote Costas loops to acquire the incoming modulated IF signal. This scheme is better than bringing the various IF signals back to the base station because those signals are weaker and would cause degradation in the phase comparisons. On the other hand, an amplified reference $r(t)$ can be sent out to stations. However, this present scheme requires a phase comparator in each remote terminal. The results expressed in 5 bit words are sent back together with the element address. The latter would not be needed if wire communications is used.

Back at the base reference, various information as shown in Figure 2.9 is assembled as a packet preceded and followed by a preamble and postamble respectively. This is shown in Figure 2.10. The frequency information (to the nearest 100Hz) is needed in both the surveying and source location computations. Since f_{PS} is one of the 300 bands and f_1 lies in one of the 1000 filter bandwidths, at least 19 bits of data are needed. No word synchronizer is built into the satellite because this information is of secondary importance and can be extracted after the source coordinates are computed. Moreover it saves on hardware on the satellite. Consequently most of the binary information from the earth-borne source in Figure 2.10, including its header, is relayed to the ground station and this exceeds the source address which is only 20 bits wide. Much more allowance must be provided since the position of the header is unknown. About 50-60 bits, which covers two full lengths of header and source code, should suffice. Each element address can be coded into $\log_2 N = 5$ bits for N about 20. So the address and phase information requires 200 bits in all, making a total of about 300 bits including 20 bits preamble and 10 bits postamble of all zeros. It should be noted that many tradeoffs could be conducted to optimize the system. For example the choice of 1000 narrow band filters and envelope detectors may be improved by using 10-coarse and 100-fine detectors. However, this was beyond the scope of the present effort.

CW	P1	P2	Freq.	Source Addr.	Elem.1 Addr.	Phase 1		Phase N	Postamble
----	----	----	-------	--------------	-----------------	---------	--	------------	-----------

Preamble

CW : For carrier recovery, about 0.6 sec
P1 : Alternate +1, bit sync 10 bits
P2 : Word Sync, 11 bit Barker sequence
Freq : 19 bits
Source Address: 60 bits
Element Address
and Phase : $(5 + \log_2 N)N$ bits
Postamble : 10 bits of -1's

FIGURE 2.10 DOWNLINK FRAME FORMAT

CW	P1	P2	Address	P1	P2	Address	P1	P2	Address	CW
----	----	----	---------	----	----	---------	----	----	---------	----

CW : 0.5 sec
P1 : 10 bits + 1 3 blocks \approx 0.25 sec
P2 : 11 bits Barker at 500 bps rate
Address : 20 bits

FIGURE 2.10 FORMAT OF SOURCE TRANSMISSION

The first half can be alternate +1's for bit sync and the second half is a Barker **sequence** for word sync.

The bit streams are clocked into the multiplexer at their own rates but the output is a single serial bit stream at rate f_o . As in Figure 2.11, this is low-pass filtered to reduce the required bandwidth and then biphasic modulated with a subcarrier prior to down-conversion at about 1.5GHz.

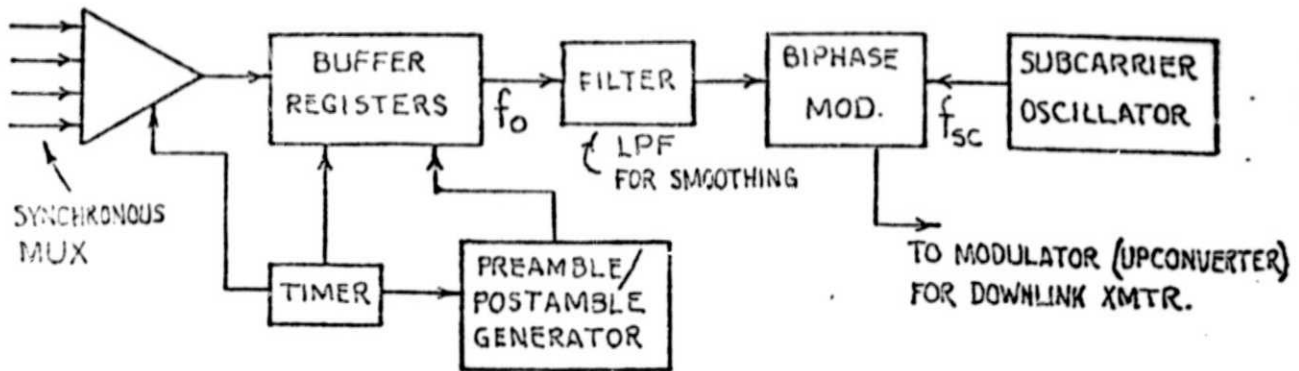


FIGURE 2.11 DOWNLINK SYSTEM

Earth Station

The requirements on the amount of information to be transmitted to ground is minimal but it is crucial that time delays be minimized. For this reason, highest priority must be assigned to this if any form of resource sharing is

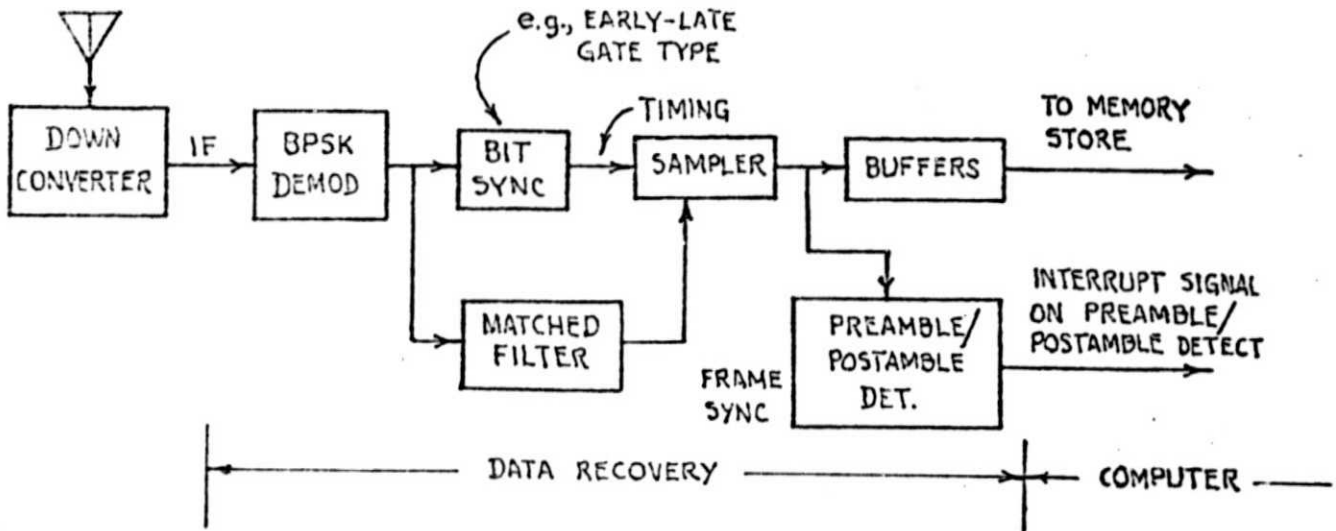


FIGURE 2.12 EARTH STATION ELECTRONICS.

required. Alternatively it could be a dedicated channel (like SCPC) which is activated on demand. We shall leave the up/down link design aside since it depends on current technology.

On down-conversion, the bi-phase modulated signal is demodulated by a Costas loop which does both carrier recovery and demodulation. The baseband

digital data are bit synchronized with an early-late gate type circuit, for example and clocked into buffers and hence into the computer after the preamble has been recognized, as shown in Figure 2.12. The data bits ought to be transferred as soon as possible and the buffer is primarily a temporary store in case of delays. A postamble stream of zeros signifies end of transmission. In the case of surveying the processor has to wait until all M sets of transmission have been received before any calculations can be made. The computer can distinguish beacons from sources by their frequency f_F . Calculations of the bit error probability of the downlink data transmission are given in [6].

Computational Requirements

We shall assume that a large computer shared with other users is available. But highest priority must be given to our application. A minicomputer is not as efficient because the accuracy requirements demand at least a 20 bit representation of the angle information (about 10^{-5} rad) while minicomputers are by definition at most 16 bits wide. Of course, double precision could be used on a mini but it would be too time consuming. Moreover, cycle times in a mini are usually larger than for a regular large computer.

The computer is used to:

(1) Survey and track the element positions as they drift in space due to gravitational forces, solar wind pressure, etc. This involves (a) an initial search over the whole region after deployment, (b) periodic surveying to track the elements, (c) locating elements just before computing the source location when a caller is detected based on pre-and post-surveys. The latter ensures up-to-date information of the elements.

(2) Use the phase information to locate earth-borne sources involving (a) a search for azimuth and elevation in satellite coordinates, (b) conversion to earth coordinates.

The surveying procedure is controlled by logic on board the satellite and is summarized in the state diagram in Figure 2.13. The computer waits for appropriate information from the satellite for data processing. Its operation is pictured in Figure 2.13.

ORIGINAL PAGE IS
OF POOR QUALITY



FIGURE 2.13(a) STATE DIAGRAM AT SATELLITE

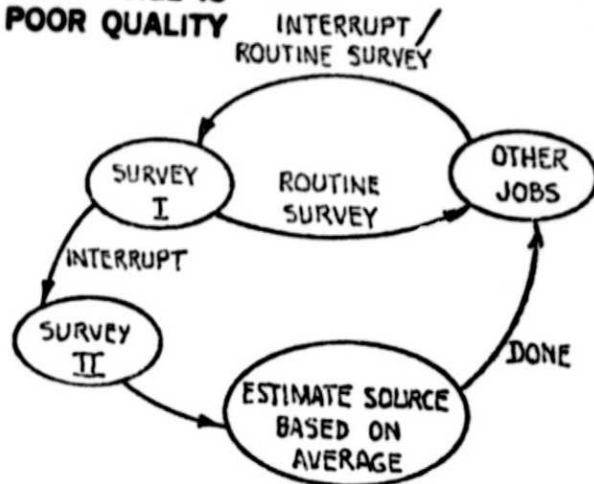


FIGURE 2.13(b) COMPUTER USAGE

The survey algorithm is described in detail in [2], while the algorithm for computing the azimuth and elevation of the caller is described in Section (2.3.2). Figures 2.14 a and b summarize both algorithms and are presented for purposes of estimating computation time.

Since the time taken to transform θ, ϕ from satellite to earth coordinates would be much less than that required to search for θ and ϕ , they are neglected here.

For the implementation of the survey, we will consider the steady-state tracking mode, since the initial search is only made once (unless the element drift is severe). At first a search over $\pm 5\lambda$ about the previous coordinate values for each of x, y and z is made with a grid size $\Delta x_1, \Delta y_1,$ and Δz_1 of 2λ . This grid implies that $F_1(s)$ has to be evaluated 125 times. Subsequently a grid of size $\frac{\lambda}{2}, \frac{\lambda}{5}$ and $\frac{\lambda}{10}$ respectively is taken. All of the above would amount to approximately 320 evaluations of $F_1(s)$, and based on previous estimates this would require about 40 seconds of computing time.

The source location technique, using the procedure outlined in [2], takes about $1000[600 \times 20] \mu\text{sec} \approx 12 \text{ sec}$ for $N = 20$ elements.

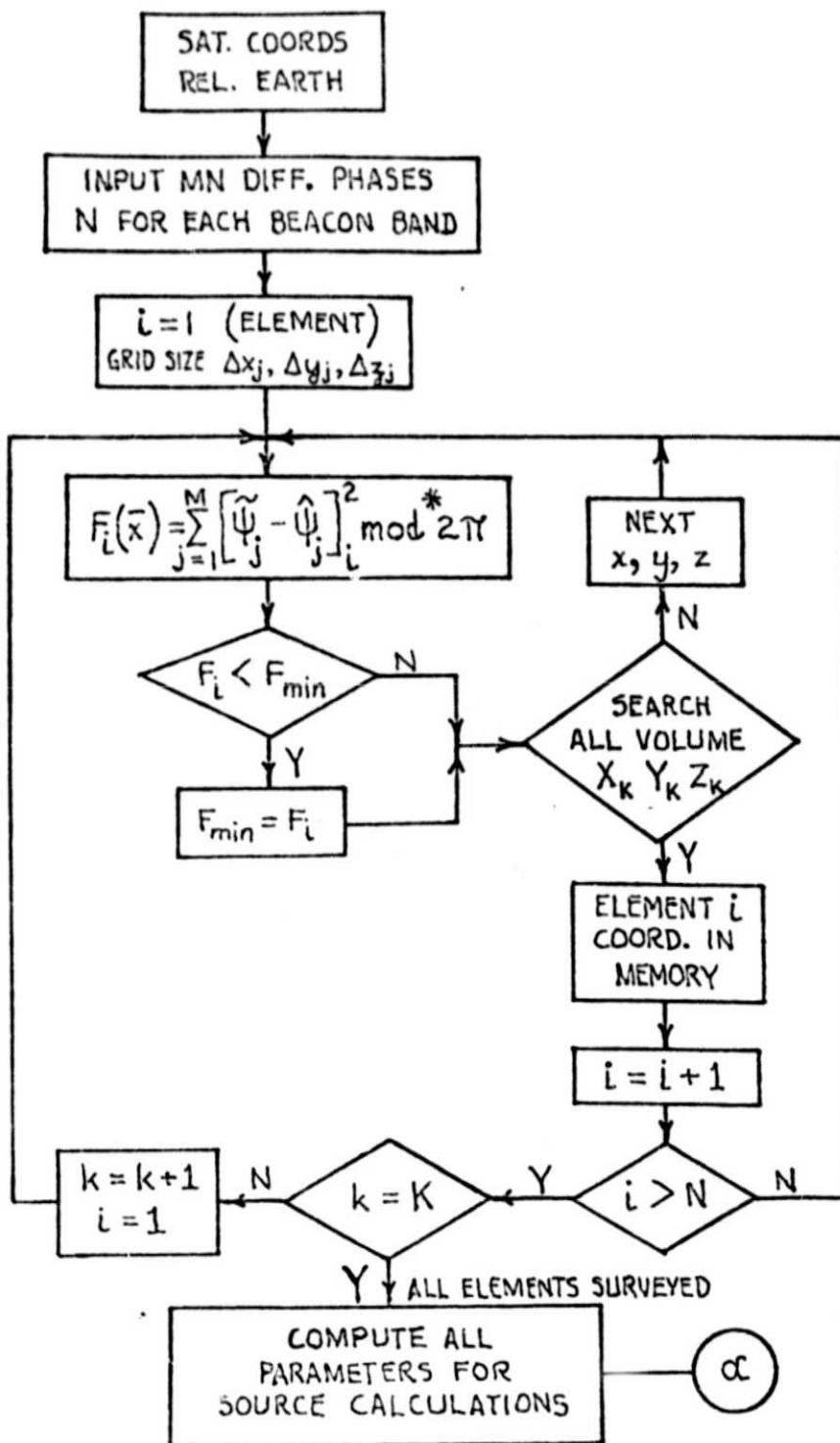


FIGURE 2.14(a) SURVEY FLOW CHART

It is seen that these computation times are large. Moreover if in the survey each frequency step is 1 second in duration, there is a delay of $M = 15$ seconds for all the phase information to reach the computer. Hence a survey takes at least 55 seconds. The 15 seconds could be reduced if less integration time is used in the phase measurements on the satellite. A faster computer could be used. It is because of this problem that the scheme shown in Figure 2.13 is used.

Unresolved Problems

- 1) the large amount of computation time required especially in surveying which exceeds delay and data transfer times.
- 2) availability of accurate earth-satellite coordinate relationship at the instants of time that the corresponding phase measurements are made.
- 3) motion of the elements during the phase measurements.
- 4) maintaining the orientation of the antennas so that they face the earth at all times.
- 5) effect of multipath (which might degrade the system).
- 6) effect of scintillation and refraction in the atmosphere.

Conclusion

The electronic and signal processing system is feasible. The more expensive items in the satellite are the frequency synthesizer, the phase comparators and the Costas loops which are assumed available at the respective operating frequencies at nominal prices. Power amplifiers are needed to pipe LO signals to the remote elements.

The demand on bandwidth is minimal and the earth station signal processing hardware is of the same form as that in the satellite.

2.4 THE THIRD SYSTEM CONCEPT: THE SIMULTANEOUS TRANSFORM ARRAY

In this section a new array concept called the Simultaneous Transform Array is introduced, which may be referred to as the third system concept for this array in space. Although the second system concept has been found satisfactory, it is felt that this new concept should also be considered as a viable alternative which may lead to a better design.

The new array system operates in a manner analogous to an optical lens or parabolic mirror[7]; either of these devices will form an image of all the points in a region about their major axis of symmetry simultaneously rather than point-by-point as in the case of beamforming and scanning arrays. The optical lens or mirror introduces the appropriate set of phase shifts (delays) to convert the planar wavefront from a far-field point source into the quadratically shaped wavefront required to image the point source at an arbitrary focal point. When this is accomplished, points in the vicinity of the distant source can be imaged on a surface placed in the vicinity of the focus. The simultaneous transform array will function in a similar fashion. The array elements will phase-shift an impinging target wavefront so as to focus it on an energy-detecting image surface. The entire target image will be recovered from the image surface rather than through the point-by-point manipulation of array element outputs.

Figure 2.15 shows a schematic representation of how a microwave simultaneous imaging system might be implemented. Each of the array

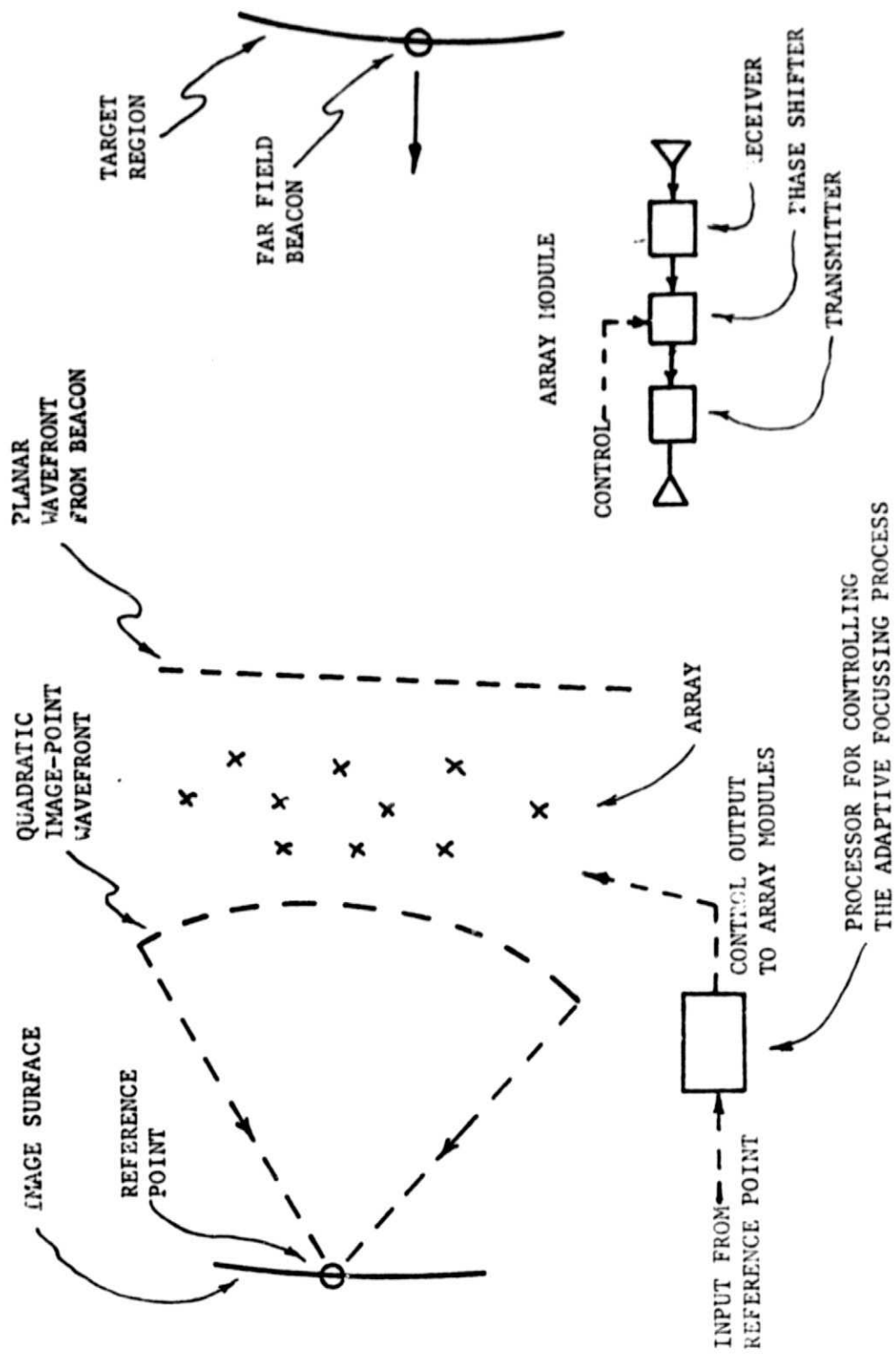


FIGURE 2.15 SIMULTANEOUS TRANSFORM ARRAY

elements can detect energy arriving from the target region. The individual array elements amplify the detected signals, phase shift them and then retransmit the signals toward the image surface shown at the left in Figure 2.15. If the appropriate phase shifts have been introduced to focus the target regions on the image surface, the energy distribution across the surface will be a microwave image of the target region.

The image surface might be made up of any of the devices which are suitable for detecting microwave energy such as gas-tube detectors, small dipoles, or fluorescent chemicals. (Much important work has been done at the Moore School with gas-tube detectors for microwave and millimeter wave holography [8]. A major factor in the choice of an energy detecting device will be the manner in which the image is to be recovered, e.g., whether it is to be viewed optically or converted into electrical signals for subsequent processing.

The image plane will contain a receiver at its center which will transmit to a central processor the signal from a point-source beacon in the target region. The central processor will adjust each of the array element phase shifters to maximize the signal observed at that receiving point. Such a technique is a modification of the beamforming procedures which have been studied at VFRC.

Once the adaptive focusing is complete the simultaneous transform array can function in a manner analogous to that of a lens. An off-axis target will produce a wavefront at the array that is slightly

tilted relative to that of the beacon. The tilted phase front will be transferred through the array modules and will produce a similar tilt in the wavefront transmitted to the image surface. Thus the target point will be displaced in the image surface from the reference beacon by the angular distance between the target and the adaptive focusing beacon in the target plane. All other targets will be similarly imaged.

A remarkable feature of the simultaneous transform array is the freedom of positions of the array elements and the lack of required knowledge of these positions. A second advantage is the elimination of the need for an image-forming signal processor. The primary disadvantage is the need for an image surface. The ultimate merit of the simultaneous array concept will depend upon the particular application. In the following section two space applications are considered. These applications are suggested as vehicles for exploration of the first order properties of the Simultaneous Transform Array (STA) concept.

Both applications to be described employ an array in space. The first is a somewhat "conventional" surveillance or measurement application; a large array is used to obtain a high resolution image of the earth for such purposes as resource studies, or volume cells in the atmosphere for meteorological purposes. The STA concept is independent of wavelength; it would permit high resolution imagery using relatively long wavelengths such as L-band, or it could work at much higher frequencies according to the detailed application, since the positional distribution of the array elements would not be a performance factor. In this type of application, the array will perform the function of a

microwave mirror and the image surface will be placed between the array and the target region.

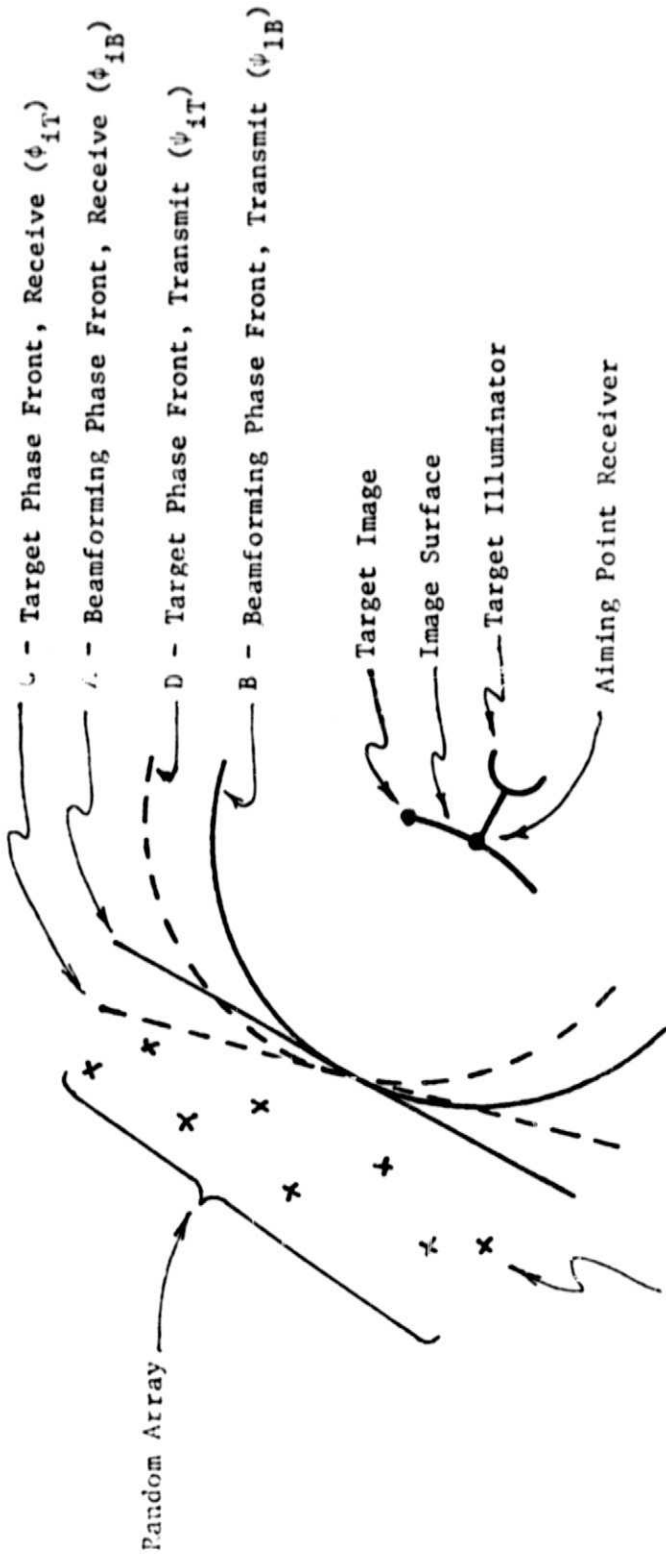
The second example treats the array as a microwave lens. In this form the STA would be useful as a deep space radio telescope. This example will introduce some other attractive characteristics of the STA concept.

2.4.1 EARTH-VIEWING RADAR

Consider an array of elements distributed randomly over a region of space; a lenticular cloud of array elements situated in a synchronous orbit 40,000 km from the earth, as illustrated in Figure 2.16 is an example. Assume that a beacon is placed on the surface of the earth to serve as a beamforming point. The signals received at the array elements are cophased, forming a radiation pattern having a main lobe in the direction of the beamforming beacon. The cophasing is accomplished with the adaptive beamforming techniques developed at VFRC, which involve measurement of the phase angles ϕ_{iB} at the array elements relative to a local phase reference when the array is illuminated by the earth beacon.

(In Figure 2.16 , a planar phase front (A) is shown at the array due to the beacon, implying that the Earth is in the far field of the array, which is not a necessary condition.)

A second beamforming process is accomplished by the same array modules. A transmit beam pattern is formed directed at a nearby image surface. The surface contains an aiming point receiver. The receiver and the image surface might be located on a satellite situated



i th Array Element
Phase Quantities:

	Receive	Transmit
Beamforming	ϕ_{iB}	ψ_{iB}
Target	$\phi_{LT} =$ $\phi_{iB} - \Delta_i$	$\psi_{iB} - \Delta_i$ $= \psi_{iT}$

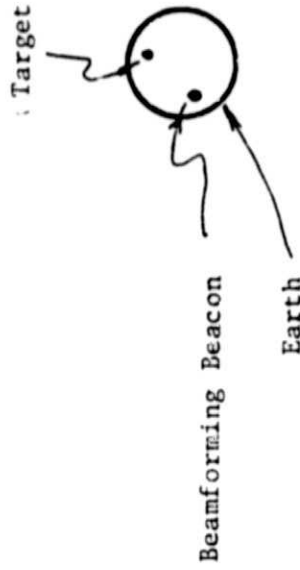


FIGURE 2.16 EARTH VIEWING RADAR

between the array and the Earth. The S/N ratio at the aiming-point receiver can be made high because the distance is short (perhaps 1 to 10 km). Also the position of the receiver with respect to the array is relatively stable. With these characteristics a transmit beamforming phasefront (B) can be obtained by feeding back from the aiming-point receiver to the array modules phase correction information to each array element; this procedure might require considerable time but since it is required only occasionally, this does not appear to present a problem.

Each array element thus stores two phases, ϕ_{iB} and ψ_{iB} , the latter being the phase correction which must be added to the local array-phase-reference to produce the quadratic phase front (B) required to focus the array on the near-field aiming point receiver.

If the beamforming beacon is now turned off and the Earth is illuminated by a radar transmitter as indicated in Figure 2.16, target reflections will be obtained. A strongly reflecting point on the Earth would produce the tilted phase front (C) shown in Figure 2.16. The array modules would measure phase angles ϕ_{iT} . The phase difference between the stored beamforming angle ϕ_{iB} and the measured target angle ϕ_{iT} is Δ_i . Δ_i will be computed and subtracted from the transmit beamforming angle ψ_{iB} to form the new target transmit phase. The result is a tilted quadratic transmit phase front (D) causing the transmit beam to image the target at a point displaced from the aiming-point receiver.

To observe and recover the target image it is necessary to surround

the aiming-point receiver by a detection surface consisting of an array of energy detectors which may be scanned or read out sequentially. The image surface might consist of an array of dipoles and detectors, gas tube RF detectors, or any other transducer which produces an output proportional to impinging RF radiation. It should be noted that these detectors do not have to be particularly sensitive as they are not responding to the low level return from the Earth target; instead they are being illuminated by the relatively near-by array elements which detect and amplify the low-level Earth signals to produce arbitrary power levels at the image surface. In this way the random array functions as a microwave mirror, simultaneously transforming the Earth-region into an image on the nearby image surface without the necessity of point-by-point scanning of the array beam pattern.

Geometric distortions will arise as in any other diffraction system; as the angular extent of the target region increases and/or the distance from the array to the image plane is reduced, the distortion will increase. Increasing the distance between the image surface and the array decreases the distortion but increases the size of the image surface. Reducing the area of view or using several Earth beacons which could be selectively activated also reduces the distortion and permits a smaller image surface without loss of resolution. Thus there is a number of system parameters which interrelate and which might be used to reduce the distortion and/or limit the size of the image plane.

Another solution might be to structure the array as a collection of subarrays each of which is limited in size so that both the target region and the image surface are in its far field and the transmit and

receive wavefronts are both linear. The quadratic transmit wavefront required of a high magnification array would be approximated by a series of planar wavefronts, one from each subarray. In still another form a subsystem would measure the element locations, the knowledge of which would permit correction for geometric distortions.

Clearly the STA concept is very flexible. A study is required to determine the best ways of utilizing the concept for particular applications.

2.4.2 RADIO TELESCOPE FOR DEEP SPACE

The simultaneous transform array concept also appears suited to the implementation of a large space-borne radio telescope. A schematic representation of such a system is shown in Figure 2.17. The array is used as a lens to image a region of small angular extent onto an image surface located on the opposite side of the array. The image surface is assumed to be relatively small; consequently the angle of view of the array is small. The image surface might be mounted on a space vehicle so that the direction of observation of the array could be changed by movement of the image surface. The distance between the array and the image surface might also be varied to control the magnification of the array. Geometric distortion will be much less significant in this application because the angle of view of the array will be small. The array will be focused in a particular direction by using a movable beacon on the image-surface side of the array. It is proposed to accomplish focusing by using a beacon frequency that is much lower than

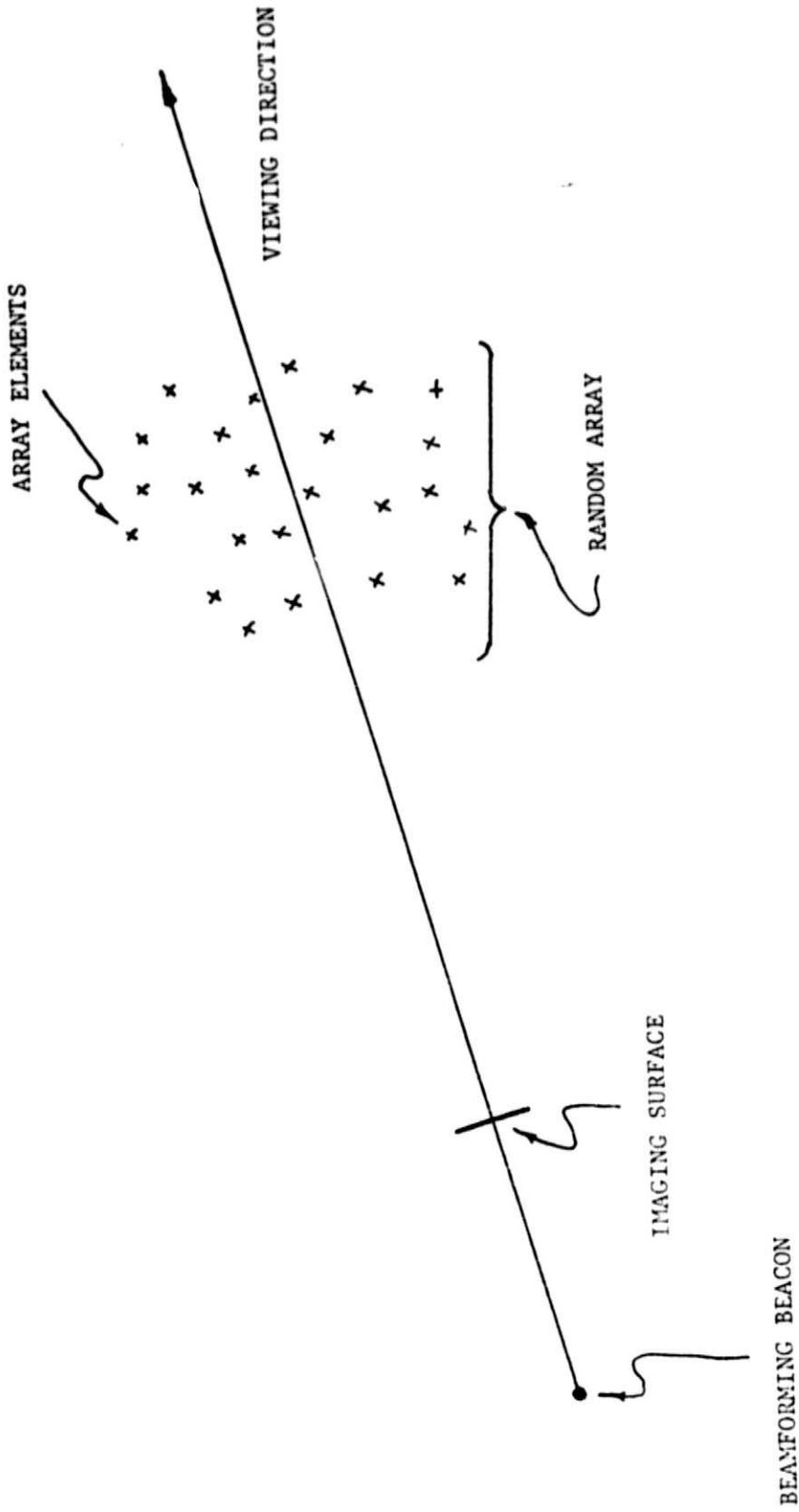


FIGURE 2.17 LARGE SPACE-BORNE RADIO TELESCOPE

that used for imaging. Use of a low frequency will permit focusing the array at infinity even though the focusing beacon is relatively close to the array. The far field focusing boundary for the array is approximately equal to D^2/λ where D is the size of the array and λ is the operating wavelength [9]. Thus by using a low beacon frequency for adaptive focusing, the far field boundary is effectively close to the array and a nearby beacon can be used for far field focusing. The use of different frequencies for reception, transmission, and focusing is yet another operating possibility which might be exploited in some applications.

The viewing direction of the radio telescope will be around the axis from the adaptive focusing beacon to the array. A logical and practical location for the beacon is on the image surface. The telescope will be aimed by physically moving the beacon and the image surface. The magnification of the array can be varied by adjusting the distance between the image surface and the array. Following selection of direction and magnification the array will then be focused by transmitting a low frequency signal from the beacon. This source will generate a wavefront which appears planar at the array. The array will use this wavefront as if it were arriving from a point source at infinity on the object side of the array. After the transmit wavefront from the array has been focused on the image surface, the focusing beacon can be turned off and the array can be used to produce high resolution images of targets in the viewing direction.

In conclusion it should be noted that the simultaneous Transform Array is different from any of the array systems which have been studied at Valley Forge Research Center, and it carries with it a new set of problems. As the examples given have suggested it has a number of important features which warrant examination. One of the most important is the concept of high resolution microwave imaging without knowledge of the locations of the array elements. This possibility alone would make the STA an important study area. Geometric distortion, measurement tolerances and system organizations need to be examined theoretically and tested experimentally.

ORIGINAL PAGE IS
OF POOR QUALITY

3. ATS-6 TO EARTH SPATIAL CORRELATION EXPERIMENT AT L-BAND

3.1 THE EXPERIMENT

The primary intent of the experiment was to obtain some measured estimate of the maximum size of a ground-based antenna array which could simulate spaceborne equipment. An array in space can be assumed to be in a transparent and stable propagation medium. Signals from the earth after passage through the atmosphere and ionosphere travel undistorted in a free-space environment to a geosynchronous array. On the other hand, the atmosphere and ionosphere are on the receiving end of a circuit from geosynchronous orbit to earth. Therefore the medium effects upon signals received on a large downlink aperture would be more severe than if the large array were in space. Experimental confirmation of any space system design must be performed on earth, however. Hence it is necessary to have some idea of the largest ground-based array which will properly simulate a spaceborne system, under different atmospheric conditions.

Since operation of the antenna array is critically dependent upon the spatial coherence of the phase of the received wave across the aperture, the experiment was set up to gather some information about this function. An equivalent quantity is the variance of the phase difference as a function of spacing between receivers. It was this quantity which was measured. The maximum baseline available for the experiment was 800 feet. It was found that the RMS fluctuation in the phase difference for all measurements was no more than the order of 1° , which is 1 to $1\frac{1}{2}$ orders of magnitude below tolerance. Hence it was concluded that an earth bound experiment with an aperture of 800 feet would be indistinguishable from one in space. It was also concluded that an array many times larger also could properly simulate a spaceborne experiment.

The second measurement was the power density spectrum of the differential phase fluctuations. Although this function bears no relation to the rationale

for conducting the experiment, it was possible to gather such information and to make the necessary calculations. It was found that the power density spectrum falls off with frequency approximately as $f^{-5/2}$.

The experiment was performed by measuring the phase difference $\Delta\phi$ between two receivers tuned to the ATS-6 geostationary satellite L-band CW emission. Specifically, the objective was to determine the differential phase as a function of distance separation between the receivers. A strongly turbulent medium would introduce large scintillations on the wave and the effect would be seen in the results as a large variance in the differential phase.

The VFRC upper site was chosen because the satellite path would be in line-of-sight of the receivers over the entire period when the satellite was in transit from approximately S70°E to its final position of S 72°W, as shown in Figure 3.1.

The receiver setup used is shown in Figure 3.2. Specifications are listed below:

1. Low noise amplifier (LNA) 10MHz BW
2. Mixer from TACAN gear: (a) 3-section filter on LO input tuned to 1508 MHz, 14MHz BW; (b) 2-section filter at RF input tuned to 1550 MHz, 20 MHz BW; (c) 42 MHz output, 4 MHz BW. There is an IF preamplifier stage also.
3. IF amplifier from TACAN gear: all tube, 42 MHz, 4MHz bandwidth.
4. In-house line driver: isolator and amplifier for 50 Ω cable driving for the IF output.
5. Local oscillator FXR Inc. Model L772A: Measured noise figure, $F = 4$ dB; overall system BW ≈ 4 MHz.
6. 4 ft. dish antenna, right circular polarized, from MARAD.

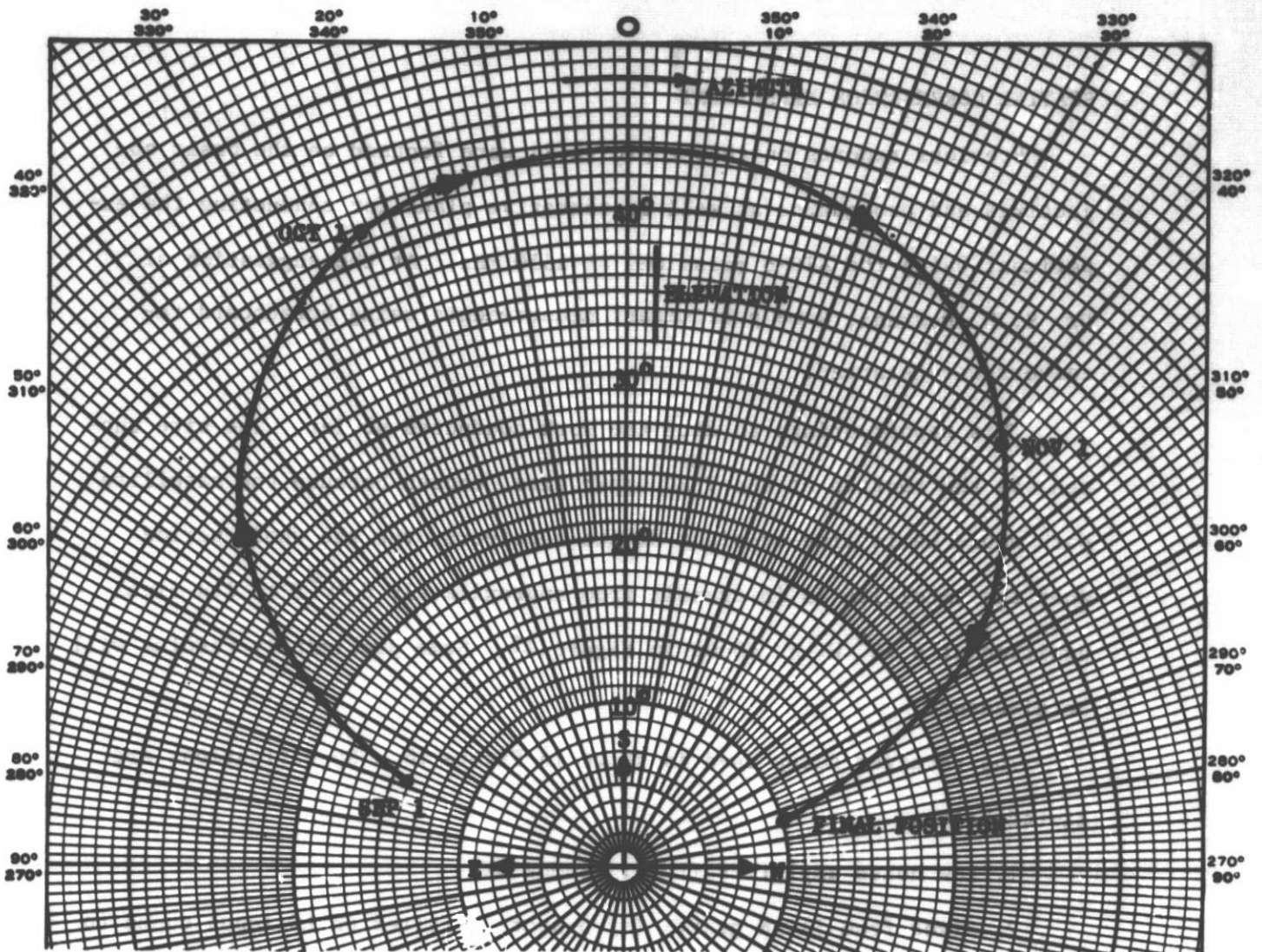


FIGURE 3.1 TRAJECTORY OF ATS-6 SATELLITE AS SEEN AT VFRG (40°N, 75°W)

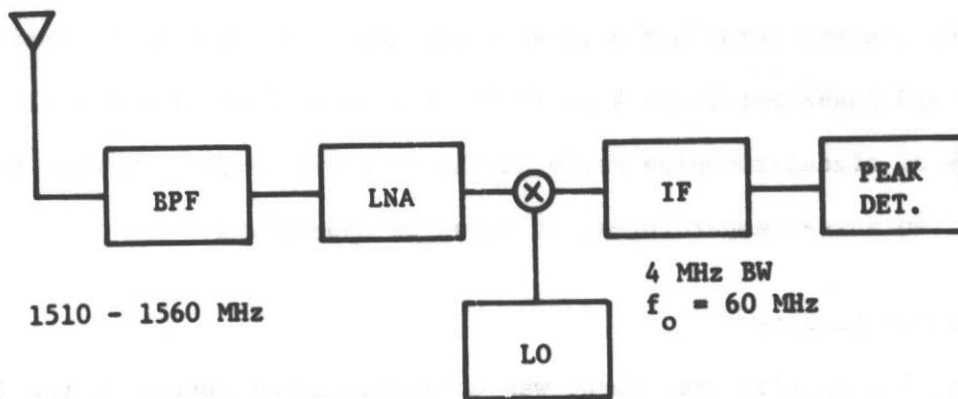


FIGURE 3.2 RECEIVER SYSTEM

Figure 3.3 shows the phase measurement setup used. For separations of 40 feet or less, no power amplifier is required for the LO signal. For larger baselines it is essential because of cable losses at 1508 MHz.

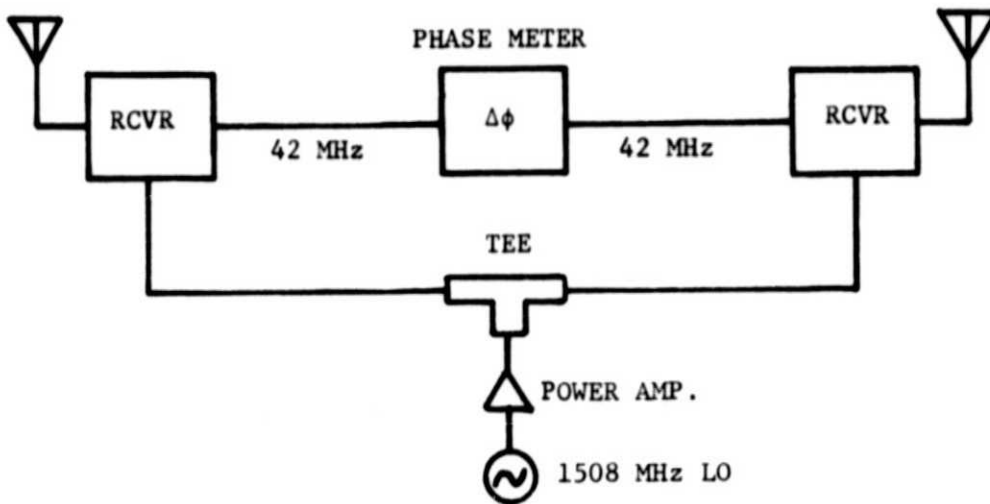


FIGURE 3.3 EXPERIMENTAL SETUP

The cables transmitting back the 42 MHz signals for phase comparisons were standard coaxial types (about 1.4 db loss per 100 ft). Special low loss cables (5 db/100 ft) were used to pipe the LO even with the power amplifier present. Owing to the absence of a power splitter at the time of the experiment, only a simple coax tee was used (which unavoidably caused some power loss). The phase meter was a HP 8405A vector voltmeter with a 1kHz bandwidth and an accuracy of about 0.1° . The result was recorded on a paper strip recorder which had about 0.3 Hz bandwidth.

The experiment was conducted mainly at ground level at VFRC for the large separations. The roof top gave a better view of the satellite, but was useful only for separations of less than 100 ft. The actual receiver separation perpendicular to the satellite, ρ , was calculated from the physical distance between the receivers and the angle between the baseline and the incoming wave direction.

For comparison with observations, a theoretical analysis of the expected output signal-to-noise ratio is made in Appendix VI. Since the satellite was in motion, we expected to observe a differential doppler as a ramp in the phase record. Appendix VII gives an example of the phase change.

3.2 RESULTS

(a) The first item of interest is the differential phase variance. As described earlier, the phase fluctuation would be superimposed on a ramp because of the satellite motion. Samples ϕ_i , $i = 1, \dots, n$, are taken from selected portions of the chart recordings free from spurious disturbances. A least square linear fit was made for each run selected. Thus $\phi = \hat{a} + \hat{k}(t - \bar{t})$ where

$$\begin{aligned}\hat{a} &= \frac{1}{n} \sum_i \phi_i = \bar{\phi} \\ k &= s_{tx} / s_{tt} \\ s_{tx} &= \frac{1}{n} \sum_i (\phi_i - \bar{\phi})(t_i - \bar{t}) \\ s_{tt} &= \frac{1}{n} \sum_i (t_i - \bar{t})^2 \\ \bar{t} &= \frac{1}{n} \sum_i t_i \\ \sigma^2 &= \frac{1}{n-2} \sum_i [\phi_i - \hat{a} - \hat{k}(t_i - \bar{t})]^2\end{aligned}$$

Results are presented in Table 3.1 for the runs made. It is seen that the runs phase difference fluctuation is less than one degree on the average. A typical chart record is given in Figure 3.4 and an average run is about 1 to 2 minutes.

In computing the differential phase variance, we needed to consider the contribution due to random noise. It was assumed that it is equal to $1/\text{SNR}$, where SNR is the signal-to-noise ratio at the input to the phase meter.

Table 3.1 gives the observed SNR of the receiver at IF as estimated

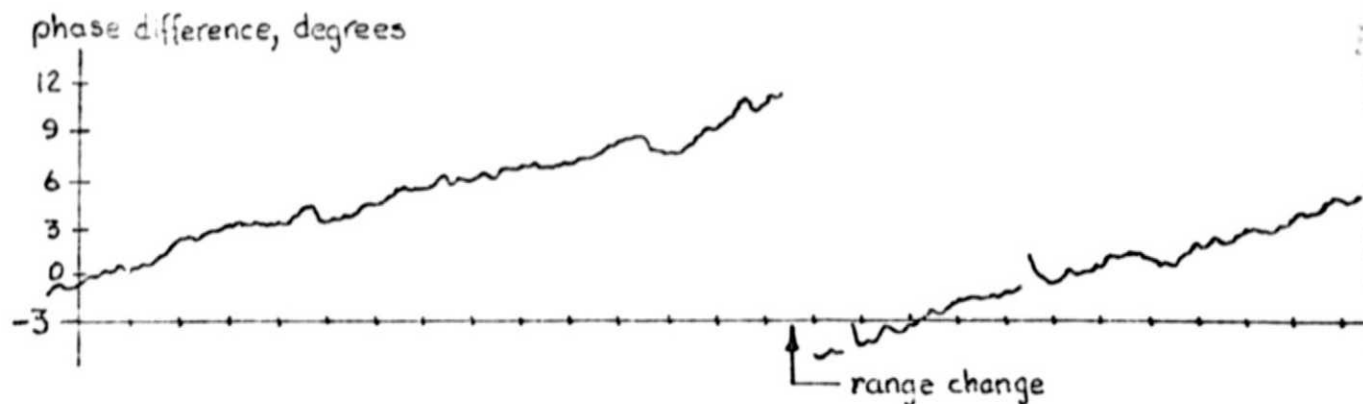
ORIGINAL PAGE IS
OF POOR QUALITY

FIGURE 3.4 CHART RECORDER TRACE OF DIFFERENTIAL PHASE

on the oscilloscope. The phase meter used, however, further narrows the effective bandwidth to 1 kHz from the 4 MHz in the receivers used. Thus there is an improvement of 36 dB over the receiver output. Towards the latter part of the table the SNR was quite unequal for the two receivers because one of the receivers became noisier. The value given is the smaller of the two. The last column gives the standard deviation, after correction for the noise variance ($\approx \frac{1}{\text{SNR}}$).

$$\text{Assuming } \sigma_{\phi,A}^2 = \sigma_{\phi}^2 - \sigma_{\phi,N}^2,$$

$\sigma_{\phi,A}^2$ is effective variance

σ_{ϕ} is observed variance

$\sigma_{\phi,N}$ is the variance due to random noise

it can be seen that the effect of noise is negligible for all cases since the effective SNR are all above 40 dB.

(b) An attempt was also made to estimate power spectra from the differential phase records after removing the effect of the ramp. In the

Date	Weather	Time	Separation (ft/m)	SNR(db)	Measured Variance ² (degree)	Corrected Std. Dev. (degree)
Sept. 26	windy overcast	1-2 pm	30/9	no data	~0.25	0.50
Oct. 1	windy, raining	1 - 2 am	30/9	~20	0.53	0.72
3	slight wind, after rain	3 - 4 pm	26/8	~ 20	0.27	0.51
5	slight wind overcast	6 - 7 pm	368/113	no data	2.72	1.65
15	slight wind clear	7:45-8:45 am	10/3.1	20	0.03	0.15
22	slight wind sunny	12 - 1 pm	816/251	20	0.36	0.59
27	slight wind cold	4:30-5:30 pm	751/231	17	0.34	0.57
Nov. 4	calm clear	4 - 5 pm (only partial)	640/197	9	0.29	0.43
13	windy clear	4 - 5 pm	240/79	14	0.55	0.72

-61-

ORIGINAL PAGE IS
OF POOR QUALITY

TABLE 3.1 DIFFERENTIAL PHASE MEASUREMENTS

absence of large sample sizes, the usual method of calculating the auto-correlation and Fourier transforming to the power spectrum cannot be used. The approach adopted is to compute the finite Fourier transform of the data samples using an FFT routine and then compute a smoothed periodogram, as suggested by Brillinger[10], where $s(t)$ is an integer with $\frac{2\pi s(T)}{T}$ near λ and the average is taken over $(2m + 1)$ adjacent periodograms

$$F_{\lambda\lambda}^T(\lambda) = (2m+1)^{-1} \sum_{j=-m}^m I_{\lambda\lambda}^T\left(\frac{2\pi[s(T)+j]}{T}\right), \lambda \neq 0 \text{ mod } \pi$$

where

$$I_{\lambda\lambda}^T(\lambda) = (2\pi T)^{-1} \left| \sum_{t=0}^{T-1} \exp(-i\lambda t) x(t) \right|^2$$

is the periodogram at frequency λ for a time series $x(t)$ of duration T . A theoretical basis of this technique is given in [10]

In our analysis, the value of m is chosen to be 2, i.e., the smoothed spectrum at each frequency λ is an average of 5 adjacent periodograms. The analysis was made on several runs obtained; two typical spectra obtained are given in Figure 3.5.

In both cases the power density spectra fell off as $f^{-5/2}$. The continuous line through each plot is a rough average of the computed points. Also given is the 95 percent confidence interval drawn as dashed lines. It is shown in [10] that

$$\frac{(4m+2)F_{XX}^T(\lambda)}{\chi_{4m+2}^2\left(\frac{1+\gamma}{2}\right)} < F_{XX}(\lambda) < \frac{(4m+2)F_{XX}^T(\lambda)}{\chi_{4m+2}^2\left(\frac{1-\gamma}{2}\right)}$$

for the 100 γ percentage confidence interval.

ORIGINAL PAGE IS
OF POOR QUALITY

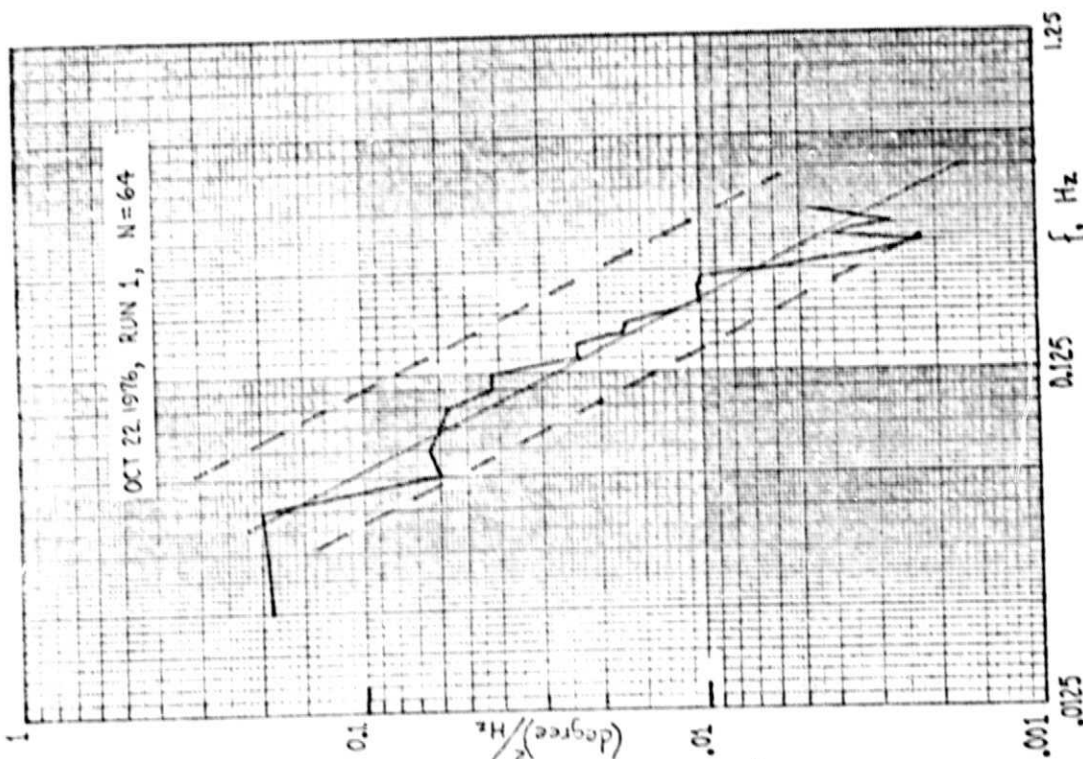
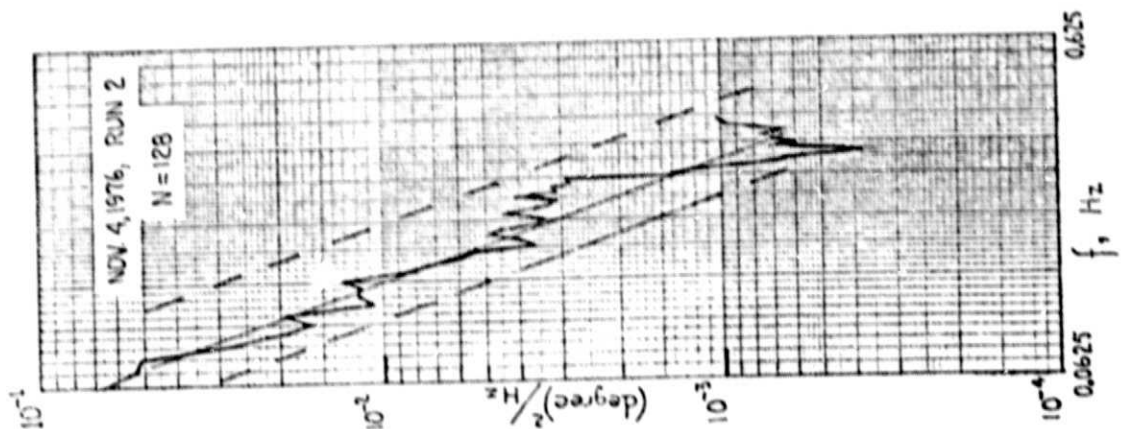


FIGURE 3.5 POWER SPECTRUM OF THE DIFFERENTIAL PHASE

ORIGINAL PAGE IS
OF POOR QUALITY

ORIGINAL PAGE IS
OF POOR QUALITY

3.3 THEORETICAL INVESTIGATION

A great deal of literature exists on wave propagation through the ionosphere and troposphere, treating them as random media with fluctuating dielectric constants. In the nonionized lower atmosphere, the variation of the dielectric constant is due to winds, thermal currents, etc., while in the ionosphere, the variation is due to deviations in electron density. Much work, e.g., [11,12,13], models the ionospheric layer as a thin, phase screen. This approach allows considerable simplification in calculating statistical properties of the field. A second body of knowledge originates in investigations of optical and millimeter wave propagation through the troposphere. Some review articles are [14,15,16]. Experimental results have been reported in [17,18] for tropospheric propagation. Considerable effort has been given in applying the multiple-scatter technique to trans-ionospheric problems in the equatorial and auroral regions where strong scintillations have been observed [19]. It has also been reported, e.g., [20], that at radio frequencies in the GHz range the fluctuations in the wave are due primarily to the ionospheric irregularities. The most recent paper [22] provides both theoretical and experimental results of amplitude and phase scintillation caused by the ionosphere and appeared only after our experiment was completed.

The objective of this study is to confirm the magnitude of phase difference fluctuations observed in the experiment described earlier. At this latitude, the ionosphere is relatively quiet and since the satellite is in line-of-sight of the receivers, there is a strong specular component. Consequently the single scatter approach will be used, as treated in [21].

Following Tatarski [21], we shall assume the wavelength λ is much less than the inner scale of turbulence in order to simplify the calculations. In so doing, the scalar wave equation instead of the vector equation can be used. This assumption also means the effective scattering cone is small and results in considerable simplification. It has been shown in [23] that most of these results at optical frequencies can be extended to microwave frequencies. Starting with the wave equation, and $\bar{E} = E_x e^{ikz} \hat{x}$, for linear polarization,

$$\nabla^2 \bar{E} + \nabla(\bar{E} \cdot \nabla \epsilon_r) + k_0^2 \epsilon_r \bar{E} = 0, \quad k_0^2 = \omega^2 \mu_0 \epsilon_0 \quad (3.1)$$

The above assumption reduces the problem to solving the scalar equation

$$\frac{\partial^2 \psi_1}{\partial x^2} + \frac{\partial^2 \psi_1}{\partial y^2} + 2ik \frac{\partial \psi}{\partial z} = 0, \quad k^2 = k_0^2 \epsilon_r \quad (3.2)$$

where $E_x = E_{ox} + E_{lx}$, $E_{lx} \ll E_{ox}$

Also $E_x \hat{x} \triangleq A e^{is} = e^{\psi_0 + \psi_1}$

$$\psi_1 = E_{lx}/E_{ox} = \chi + iS_1$$

χ and S_1 are the log-amplitude and phase departure of the perturbation term E_{lx} caused by scattering in the random medium.

From (3.2) it has been shown (section 7.3 of [21]) that the phase structure function $D_S(\rho)$ can be derived:

$$D_S(\rho) \Big|_Z = E\{|S_1(x, y, Z) - S_1(x', y', Z)|^2\} \quad (3.3)$$

$$= 4\pi \int_0^\infty [1 - J_0(k\rho)] F_S(\kappa, 0) \kappa d\kappa \quad (3.4)$$

where $\rho = \sqrt{(x-x')^2 + (y-y')^2}$ is the antenna separation which is assumed

to be less than L_0 , the outer turbulent scale. In writing 3.4 we have assumed locally homogeneous fields,

$$f(\bar{r}) = f(0) + \iiint (1 - e^{i\bar{\kappa} \cdot \bar{r}}) d\phi(\bar{\kappa}) \quad (3.5)$$

where $d\phi(\bar{\kappa})$ is a random amplitude satisfying

$$E\{d\phi(\bar{\kappa}_1) d\phi^*(\bar{\kappa}_2)\} = \delta(\bar{\kappa}_1 - \bar{\kappa}_2) \phi(\bar{\kappa}_1) d\bar{\kappa}_1 d\bar{\kappa}_2 \quad (3.6)$$

and also local isotropy,

$$D_f(\bar{r}) = E\{|f(\bar{r} + \bar{r}_1) - f(\bar{r}_1)|^2\} = D_f(|\bar{r}|) \quad (3.6)$$

Details are given in Tatarski's first book, Chapter 1 and 7. In (3.4), the term $F_s(\kappa, 0)$ is the two-dimensional spectral density of the structure function of the phase fluctuation in the plane $z = Z$. As in Chapter 8 in the book, it is related to the refractive index spectral density

$F_\epsilon(\kappa_1, \kappa_2, |z' - z''|, \frac{\bar{r}' + \bar{r}''}{2})$ by

$$F_s(\kappa, 0) = \frac{k^2}{4} \iint_0^Z \cos\left[\frac{\kappa^2(Z-z')}{2k}\right] \cos\left[\frac{\kappa^2(Z-z'')}{2k}\right] F_\epsilon(\kappa, |z' - z''|, \frac{\bar{r}' + \bar{r}''}{2}) dz' dz'' \quad (3.7)$$

$$\kappa^2 = \kappa_1^2 + \kappa_2^2$$

F_ϵ is in general a function of the separation of the two points of interest, $z' - z''$, and can vary along the path from 0 to Z . Thus assuming there are n layers each with a spectral density $F_{\epsilon i}$, from (3.7)

$$F_s(K, 0) = \frac{k^2}{4} \sum_{i=0}^{n-1} \iint_{z_i}^{z_{i+1}} \left[\cos\frac{K^2 \xi}{2k} + \cos\frac{K^2(Z-\eta)}{2k} \right] F_{\epsilon i}(K_1, K_2, k\xi, \frac{\bar{r}' + \bar{r}''}{2}) dz' dz'' \quad (3.8)$$

$$\xi = z' - z'', \quad \eta = (z' + z'')/2$$

$$z_0 = 0, \quad z_n = Z$$

This is an extension of the results in [21], Chapter 8, where the irregularities are correlated only within each layer. Now assume $F_{\epsilon i}$ can be written as

$$F_{\epsilon i}(\kappa_1, \kappa_2, \xi, \frac{r'+r''}{2}) = C_n^2(\frac{r'+r''}{2}) f_{\epsilon i}(\kappa_1, \kappa_2, \xi) \quad (3.9)$$

From (3.8) the double integral can be rewritten as

$$\int_{z_i}^{\frac{z_i+z_{i+1}}{2}} C_n^2(\bar{r}) d\eta \int_{-2(\eta-z_i)}^{2(\eta-z_i)} f_{\epsilon i}(\kappa_1, \kappa_2, \xi) [\cos \frac{\kappa^2 \xi}{2k} + \cos \frac{\kappa^2 (Z-\eta)}{k}] d\xi \quad (3.10)$$

$$+ \int_{\frac{z_1+z_{i+1}}{2}}^{z_{i+1}} C_n^2(\bar{r}) d\eta \int_{2(\eta-z_{i+1})}^{-2(\eta-z_{i+1})} f_{\epsilon i}(\kappa_1, \kappa_2, \xi) [\cos \frac{\kappa^2 \xi}{2k} + \cos \frac{\kappa^2 (Z-\eta)}{k}] d\xi$$

As in Chapter 8 of [21] if $\kappa \xi \ll 1$, $\kappa^2 \xi/k \ll 1$ and $2(\eta-z_i)$, $-2(\eta-z_{i+1})$ are of magnitude $(z_{i+1} - z_i)$, the inner integrals of both terms in (3.10) are approximately

$$2[1 + \cos \frac{\kappa^2 (Z-\eta)}{k}] \int_0^\infty f_n(\kappa_1, \kappa_2, \xi) d\xi = 4\pi \phi_{\epsilon i}^0(\kappa) \cos^2 \left[\frac{\kappa^2 (Z-\eta)}{2k} \right]$$

$\phi_{\epsilon i}(\kappa)$ is the 3-dimensional spectral density of the i^{th} medium so

$$F_s(\kappa, 0) = \frac{\pi k^2}{2} \sum_{i=0}^{n-1} \int_{z_i}^{z_{i+1}} C_n^2(\bar{r}) \phi_{\epsilon i}^0(\kappa) \cos^2 \left[\frac{\kappa^2 (Z-\eta)}{2k} \right] d\eta \quad (3.11)$$

If however, $C_n^2(\bar{r})$ is constant within each layer, we can expand the inner integral as in Chapter 7 of [21] instead.

$$\begin{aligned}
 & \int_0^{z_{i+1}-z_i} d\xi \int_{z_i+\xi/2}^{z_{i+1}-\xi/2} \left[\cos \frac{\kappa^2 \xi}{2k} + \cos \frac{\kappa^2}{k} (Z-\eta) \right] F_{\epsilon i}(\kappa, 0) d\eta \\
 & + \int_{-z_{i+1}+z_i}^0 d\xi \int_{z_i-\xi/2}^{z_{i+1}+\xi/2} \left[\cos \frac{\kappa^2 \xi}{2k} + \cos \frac{\kappa^2}{k} (Z-\eta) \right] F_{\epsilon i}(\kappa, 0) d\eta \\
 & = (z_{i+1}-z_i) + 2 \left(\cos \frac{\kappa^2}{k} \left(Z - \frac{z_i+z_{i+1}}{2} \right) \sin \frac{\kappa^2}{2k} (z_{i+1}-z_i) \right) \frac{k}{\kappa^2} \quad (3.12)
 \end{aligned}$$

Equation 3.8 reduces to

$$\begin{aligned}
 F_s(\kappa, 0) &= \frac{\pi k^2}{4} \sum_{i=0}^{n-1} (z_{i+1}-z_i) \left[1 + \frac{2k}{\kappa^2} \frac{1}{(z_{i+1}-z_i)} \sin \frac{\kappa^2}{2k} (z_{i+1}-z_i) \right. \\
 & \left. \cos \frac{\kappa^2}{k} \left(Z - \frac{z_{i+1}-z_i}{2} \right) \right] \phi_{\epsilon i}(\kappa) \quad (3.13)
 \end{aligned}$$

So by (3.4)

$$D_s(\rho) = \pi^2 k^2 \sum_{i=0}^{n-1} (z_{i+1}-z_i) \int_0^{\infty} [1 - J_0(\kappa \rho)] [] \phi_{\epsilon i}(\kappa) \kappa d\kappa \quad (3.14)$$

where [] is the term (3.13) within square brackets.

During its passage to earth, the wave passes through a layer of ionosphere, some free space and a thin troposphere about 10 km in height. As mentioned earlier, the tropospheric effect can be neglected unless the wave arrives at the receivers at a low elevation angle. Assuming we use (3.14) the structure function reduces to

-69-

$$D_s(\rho) = \pi^2 k^2 L \int_0^\infty [1 - J_0(k\rho)] \left[1 + \frac{2k}{k^2 L} \sin \frac{k^2 L}{2k} \cos \frac{k^2}{k} \left(\frac{z - L}{2}\right)\right] \phi_\epsilon(k) k dk \quad (3.15)$$

where $\phi_\epsilon(k) = 0$ in the free space layer.

We shall use the model given in [20]

$$\phi_\epsilon(k) = \frac{L_o^3}{\pi^2 (1 + k^2 L_o^2)^2} \langle \epsilon_1^2 \rangle \quad (3.16)$$

where $\epsilon_r(\bar{r}) = \langle \epsilon \rangle (1 + \epsilon_1(\bar{r}))$, the relative permittivity. In the ionosphere

$$\begin{aligned} \epsilon_1 &= \epsilon_o (1 - f_p^2 / f^2) - \epsilon_o (f_p^2 / f^2) \frac{\Delta N}{N_o} \\ &= \epsilon_o \epsilon_r \\ \epsilon_1(\bar{r}) &= \frac{f_p^2}{f^2} \frac{\Delta N(\bar{r})}{N_o} / \left(1 - \frac{f_p^2}{f^2}\right) \\ \langle \epsilon_1^2 \rangle &= \left\langle \left(\frac{\Delta N}{N_o}\right)^2 \right\rangle \frac{(f_p / f)^4}{[1 - f_p^2 / f^2]^2} \end{aligned} \quad (3.17)$$

Typical values are $L_o \approx 500\text{m}$, $f_p \approx 7\text{ Mhz}$,

$$\left\langle \left(\frac{\Delta N}{N_o}\right)^2 \right\rangle^{1/2} \approx 0.1$$

Rather than evaluating (3.15) directly, we shall use Tatarski's approach by calculating $D_A(\rho) + D_S(\rho)$. It can be shown, using (3.16),

$$\begin{aligned} D_A(\rho) + D_S(\rho) &= 2\pi^2 k^2 L \int_0^\infty [1 - J_0(k\rho)] \phi_\epsilon(k) k dk \\ &= 2\langle \epsilon_1^2 \rangle k^2 L L_o^3 [1 - \rho K_1(\rho/L_o) / L_o] \end{aligned} \quad (3.18)$$

where K_1 is the modified Bessel function of second kind.

$$\begin{aligned}
 D_A(\rho) &= 4\pi \int_0^{\infty} [1 - J_0(\kappa\rho)] F_A(\kappa, 0) \kappa d\kappa \\
 &= 2 \langle \epsilon_1^2 \rangle k^3 L_o^3 \left[\frac{L}{4kL_o^2} - \frac{\rho L}{4kL_o^3} K_1(\rho/L_o) - C(\rho) + C(0) \right] \quad (3.19)
 \end{aligned}$$

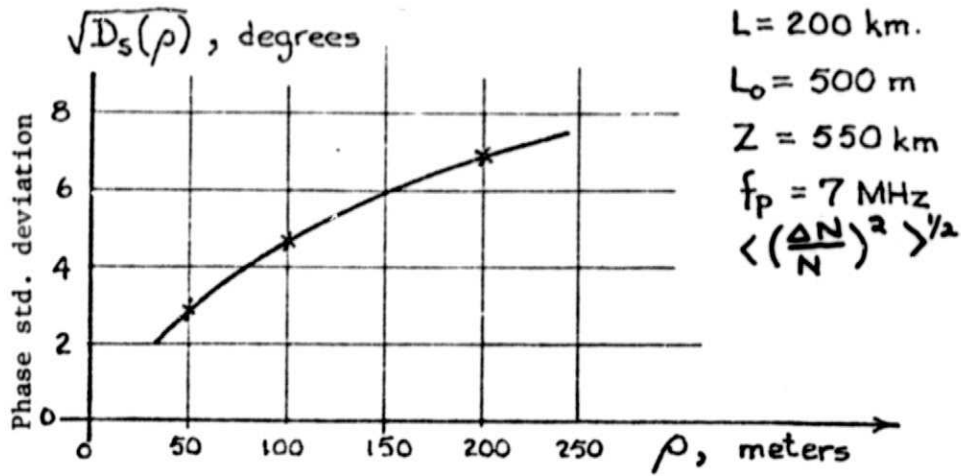
$$C(\rho) = \int_0^{\infty} \frac{1}{\kappa} J_0(\kappa\rho) \sin \frac{\kappa^2 L}{2k} \cos \left[\frac{\kappa^2}{k} \left(z - \frac{L}{2} \right) \right] \frac{1}{(1 + \kappa^2 L_o^2)^2} d\kappa$$

$D_s(\rho)$ is thus 3.19 subtracted from (3.18).

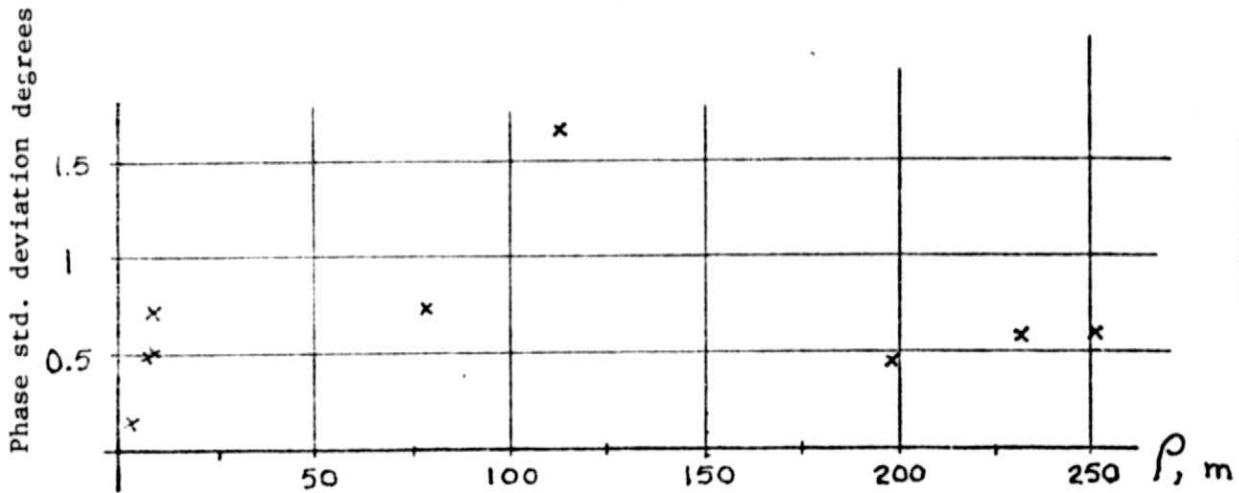
3.4 OBSERVATIONS

Equation 3.19 is integrated numerically and a typical set of results is given in Figure 3.6 for the parameters given there. The experimental results all indicate very small phase fluctuations of less than one degree standard deviation even up to 800 ft separation. It implies very strong correlation of the signal phase. It is interesting that the expected gradual increase in phase fluctuation with baseline length was not observed. If we had an extra receiver so that the phase difference between a pair close together and the other far apart, simultaneous records would allow us to make firmer conclusions. Alternatively if more time was allowed at the time of the experiment, the baseline could have been changed and the runs repeated for each baseline on the same day.

The computed results using the model of the ionosphere given show a gradual increase in phase fluctuation with separation ρ . Note however that the electron density fluctuation of 10 percent was quoted in literature discussing scintillations near the equator, which experiences much more activity than at temperate regions. As given in 3.20, if $\langle \left(\frac{\Delta N}{N} \right)^2 \rangle^{\frac{1}{2}}$ were reduced to 0.03



ANALYTICAL RESULT FOR $D_s(\rho)$



PLOT FROM TABLE ONE

FIGURE 3.6

from 0.1 instead, the predicted fluctuations would be 10 times as small as the values in Figure (3.6) which are closer to the measured values.

The frequency spectra of the phase difference appears to have slopes from -2 to -2.5. In [16], Tatarski derived the expressions for the power spectra but for the model we used as given in 3.15 and 3.16 the integral is not easily evaluated. But since the Kolomogorov spectrum used by Tatarski goes as $\kappa^{-11/3}$ while that in 3.16 is approximately proportional to κ^{-4} , the results are not expected to be too different. The theoretical power spectrum derived there predicts a frequency dependency of $f^{-8/3}$ which is quite close to that in Figure 3.5. A word of caution, however, is needed here. It must be remembered that the chart recordings are not strictly differential phase at an instant but contain a time factor owing to the plane wave arriving at an angle not perpendicular to the receiver baseline. The result for October 22 should be more realistic since the angle of arrival is about 5° with the baseline normal. The spectrum reported in [22] shows a f^{-3} relationship.

The differential phase fluctuations have been observed to be consistently small so that phase coherence can be guaranteed at least up to 800 ft in case of future experiments involving an extended random array. One possibility for future investigation is to extend the baseline to several thousand feet perhaps using radio instead of wire links between receivers.

The investigation reported above involves only the down-link situation where the wave incident on the atmosphere can be assumed to be plane. The up-link involves the propagation of a spherical wave into the atmosphere, which Fried has investigated for optical frequencies [24]. Except for different

**ORIGINAL PAGE IS
OF POOR QUALITY**

-73-

values, his formulae should apply for the transionospheric link to a geostationary satellite using microwave frequencies in analogy to the down-link case.

Porcello also discussed some aspect of an uplink propagation [25].

4. SUMMARY AND CONCLUSIONS

It has been shown that the objectives of the project, namely the feasible design of an array in space and the carrying out of a spatial correlation experiment, have been fulfilled.

For the system design part of the project, three radio camera system concepts have been described. The first one, based on the use of fixed references on the earth's surface to synchronize a randomly distributed antenna array which is in geostationary orbit, and then the array scans in the neighborhood of the synchronizing source, has been shown to be theoretically feasible, but physically impractical. This is due to the requirement that the beacons can be uniformly located on any part of the earth, which is impractical.

The second system concept which was introduced and fully developed is based on the assumption that an element location subsystem can be created consisting of beacons clustered on the land masses and randomly distributed over the small angle subtended at the antenna array by the earth. An algorithm was introduced which showed this assumption to be completely valid. Thus phase measurements at each array element due to signals transmitted from the beacons are used to uniquely determine the positions of the elements of the array. Tolerance results were also given which showed the algorithm to satisfy all of the system specifications. Assuming the positions of the array elements are known, an algorithm which is closely related to the surveying algorithm is used to locate the position of transmitting sources. Further the electronic system also was designed, and it was calculated that this system concept is physically practical and it fulfills the desired objectives.

Finally a third system concept, the Simultaneous Transform Array, was introduced. No analysis was carried out; however it is strongly felt that this new concept is a possible alternative to the second system concept if subsequent design effort discloses problems not yet uncovered.

The experimental part of the project was satisfactorily completed. The project plan called for a study of the spatial correlation of the phase of the received signal up to a distance of 800 feet. It was shown that even with up to 800 feet separation between the receivers, the standard deviation of the phase fluctuation was less than one degree. (This value is so small that it is regrettable that the project plan did not include a much larger baseline.) The results were taken over a variety of atmospheric conditions and at different times of the day. A spectral analysis on the reduced data was also attempted and on those records which were computed, the phase power spectrum showed a frequency dependence of $f^{-2.5}$, which is slightly lower than that published recently [22] which showed a f^{-3} relationship.

5. RECOMMENDATIONS FOR FUTURE EFFORT

The work to be done should be a combination of theoretical study, system design, and experimental verification of applications of large-scale, space-borne arrays. Specific topics to be considered are:

- (1) The mechanical design of large nonrigid spaceborne array systems with capabilities of internal station keeping.
- (2) Communication between the array modules and the space station (this is dependent on the particular mechanical design chosen).
- (3) The design of up-link/down-link to include radio communications from the earth to the ground source via the large array.
- (4) Anti-RFI adaptive nulling.
- (5) VFRC test of self survey and direction finding algorithms.

(For this purpose it may be possible to study the results of the experiment being conducted in the summer of 1977 at VFRC in which the four elements of an array are surveyed using a set of beacons. The survey is limited to the x-y plane only. It may be necessary to modify the experimental procedure to ascertain its applicability to the space system design.)

- (6) Breadboarding and testing of an advanced array module for the spaceborne system.
- (7) Assembly of multi-element L-band, ground based array. Self survey from ground beacons. Use array to locate airborne targets.
- (8) Design the central processor.
- (9) Generation and distribution of electric power within the array.
- (10) Analytical study of the Simultaneous Transform Array and comparative evaluation with the self-survey array system.

-77- ORIGINAL PAGE IS
OF POOR QUALITY

- (11) Experimental design of ground (and sea) transmitting systems.
- (12) Experimental design of ground receiving system.

6. REFERENCES

1. Yakov Shamash, "The Survey Problem", VFRC QPR No. 20, February 1977, pp. 70-75,
2. Yakov Shamash and Saleem Kassam, "Location of Random Array Elements Using Phase Measurements", 8th Annual Modelling and Simulation Conference. Pittsburgh, Pennsylvania, April 1977.
3. R.S. Berkowitz, "System Design Considerations and Analysis of Determination Arrays for Angle Estimation", VFRC Report 35, April 1973.
4. T.L. Lim, "Source Position Location Algorithm", VFRC Report, April, 108, 1977.
5. S.A. Kassam and M. DonVito, "Random Arrays for Source Parameter Estimation", VFRC QPR No. 19, p. 65, November 1976.
6. T.L. Lim, "Satellite and Ground Station Electronics for a Large Random System", VFRC Report #109, 1977.
7. Earl N. Powers, "Simultaneous Transform Array", VFRC QPR No. 19, November 1976, pp. 71-75.
8. N.H. Farhat and N.S. Kopeika, "A Low Cost Millimeter Wave Glow Discharge Detector", Proc. IEEE (letters), Vol 60, pp 759-760, June 1972.
9. Bernard D. Steinberg, "Principles of Aperture and Array System Design", Wiley and Sons, New York, 1976.
10. D.R. Brillinger, Time Series, Data Analysis and Theory, Holt, Rinehart and Winston, 1975.
11. B.H. Briggs and I.A. Parkin, "On the Variation of Radio Star and Satellite Scintillations with Zenith Angle", J. Atmos. Terr. Phys., 25, 1963, p. 339.
12. S.A. Bowhill, "Statistics of a Radio Wave Diffracted by a Random Ionosphere", J1. Res. NBS-D. Radio Propagation, 65D, 1961, p. 275.
13. J.V. Evans, Millstone Hill Radar Propagation Study: Scientific Results Part II. NTIS Report 782-748/8 GA, Nov. 1973.
14. J.W. Strohbehm, "Line-of-Sight Wave Propagation Through the Turbulent Atmosphere", Roc. IEEE, 8, Aug. 1968, p. 1301.
15. Yu N. Barabanenkov, et al., "Status of the Theory of Propagation of Waves in a Randomly in Homogeneous Medium", Sov. Phys. Usp. 13, 1971, p. 551.
16. V.I. Tatarski, The Effects of the Turbulent Atmosphere on Wave Propagation, NTIS Report TT 68-50464, 1971.
17. M.C. Thompson, Jr. and H.B. James, "Measurements of Phase-Front Distortion on an Elevated Line-of-Sight Path", IEEE Trans AFS-6, Sept. 1970, p. 645.

18. N.A. Armand, et al, "Antenna Investigation of a Statistically in Homogeneous Atmosphere", Radio Science 10, Jan. 1975, p. 87.
19. K.C. Yeh, et al, "A Theoretical Study of the Ionosphere Scintillation Behavior Caused by Multiple Scattering", Radio Science 10, January 1975, p. 97.
20. A.W. Wernik and C.H. Liu, "Ionospheric Irregularities Causing Scintillations of GHz Frequency Radio Signals", J. Atmos. Terr. Phys 36, 1974, p. 871.
21. V.I. Tatarski, Wave Propagation in a Turbulent Medium, McGraw-Hill, New York, 1960.
22. R.K. Crane, "Ionospheric Scintillation", IEEE Proc., February 1977, p. 180.
23. S.F. Clifford and J.W. Strohbehn, "The Theory of Microwave Line-of-Sight Propagation Through A Turbulent Atmosphere", IEEE Trans. AP-18, March 1970, p. 264.
24. D.L. Fried, "Limiting Resolution Looking Down Through the Atmosphere," JI. Opt. Soc. Am., 10, October 1966, p. 1380.
25. L.J. Porcello, "Turbulence-Induced Phase Errors in Synthetic-Aperture Radars," IEEE Trans. AES-6, September 1970, p. 636.

RELATIONS BETWEEN POINTING ANGLES FROM A SPACEBORNE ARRAY AND THE POSITIONS ON THE EARTH'S SURFACE [I.1]

The steps involved in determining the longitude ϕ_e and the latitude ψ_e of a point source radiating on the earth's surface from its direction cosines u_a and v_a measured in the array coordinate system are summarized in a concise form in Table I.1.

In the first step we calculate the direction cosines of the radiating source in the array auxiliary coordinate system $(X_{1a} Y_{1a} Z_{1a})$ from its direction cosines measured in the array principal coordinate system $(X_a Y_a Z_a)$. Then, in the second step, we use the values calculated above to determine the direction cosines of the radiating source in the earth's auxiliary coordinate system $(X_{1e} Y_{1e} Z_{1e})$. The transformation of coordinates in the third step leads to the direction cosines of the radiating source in the earth's principal coordinate system $(X_e Y_e Z_e)$. Finally, in the fourth step, one readily calculates the longitude and the latitude of the radiating source.

The array associated with the system of concern will be as large as 40000 wavelengths. A design approach which assumes that the positions of the array elements (in the array coordinate system) are exactly known is too idealistic to be of practical value for arrays of such a size. Therefore we will allow uncertainties in the array element locations and will design the system accordingly, i.e., we will use reference sources located on the earth's surface to synchronize the array. Since determination of the direction cosines assumed by a radiating source in the array

[I.1] T. A. Dzekov, "Relations between Pointing Angles from a Spaceborne Array and Positions on Earth's Surface", VFRC QPR No. 18, August 1976, pp. 81-88.

ORIGINAL PAGE IS
OF POOR QUALITY

<p>Step I</p> <p>$X_a Y_a Z_a \rightarrow X_{la} Y_{la} Z_{la}$</p>	$\begin{pmatrix} u_{la} \\ v_{la} \\ w_{la} \end{pmatrix} = \begin{pmatrix} a_{lxx} & a_{lxy} & a_{lxz} \\ a_{lyx} & a_{lyy} & a_{lyz} \\ a_{lzx} & a_{lzy} & a_{lzz} \end{pmatrix} \begin{pmatrix} u_a \\ v_a \\ w_a \end{pmatrix}$
<p>Step II</p> <p>$X_{la} Y_{la} Z_{la} \rightarrow X_{le} Y_{le} Z_{le}$</p>	$w_{le} = \frac{H(1-w_{la}^2) + w_{la}[R_e^2 - H^2(1-w_{la}^2)]^{\frac{1}{2}}}{R_e}$ $u_{le} = v_{la}(1-w_{le}^2)^{\frac{1}{2}}/(1-w_{la}^2)^{\frac{1}{2}}$ $v_{le} = u_{la}(1-w_{le}^2)^{\frac{1}{2}}/(1-w_{la}^2)^{\frac{1}{2}}$
<p>Step III</p> <p>$X_{le} Y_{le} Z_{le} \rightarrow X_e Y_e Z_e$</p>	$\begin{pmatrix} u_e \\ v_e \\ w_e \end{pmatrix} = \begin{pmatrix} e_{lxx} & e_{lyx} & e_{lzx} \\ e_{lxy} & e_{lyy} & e_{lzy} \\ e_{lxz} & e_{lyz} & e_{lzz} \end{pmatrix} \begin{pmatrix} u_{le} \\ v_{le} \\ w_{le} \end{pmatrix}$
<p>Step IV</p>	$\phi_e = \tan^{-1} \left(\frac{v_e}{u_e} \right)$ $\psi_e = \sin^{-1}(w_e)$

TABLE I.1-TRANSFORMATION OF COORDINATES FROM ARRAY'S COORDINATE SYSTEM TO THE EARTH'S COORDINATE SYSTEM

coordinate system requires knowledge of the direction cosines associated with the source which synchronizes the array, we will need a procedure by which the latter can be calculated. Such a procedure is given in Table I.2. The relations presented in the table are developed in a way analogous to that used to develop the relations in Table I.1.

As seen, determination of the longitude and the latitude of a radiating source on the earth's surface requires knowledge of the geocenter to array distance (H), the radius of the earth (R_e) and the transformation coefficients* used in step I and step III in Table I.1 or in step II and step IV in Table I.2. The accuracy of position determination is very much dependent on the accuracy by which the transformation coefficients are known. Precise knowledge of the transformation coefficients is of substantial importance especially for a system which is expected to provide as high accuracy in position determination as that of the system we are concerned with.

It is unreasonable to assume that the orientation parameters of the array will coincide exactly with the parameters planned before launching; moreover it is very likely that the orientation of the array will be time dependent. Hence, we must be concerned with the problem of how one can calibrate the system, or in other words, how one can calculate (recalculate) the transformation coefficients when necessary.

Calculation of the transformation coefficients is equivalent to establishment of the two auxiliary coordinate systems ($X_{1a} Y_{1a} Z_{1a}$ and $X_{1e} Y_{1e} Z_{1e}$) the properties of which were described in the first part of the

*The transformation coefficients in essence describe the orientation of the array with respect to the earth and the angular position of the array in the earth's coordinate system.

<p>Step I</p>	$u_e = \cos\psi_e \cos\phi_e$ $v_e = \cos\psi_e \sin\phi_e$ $w_e = \sin\psi_e$
<p>Step II</p> <p>$X_e Y_e Z_e \rightarrow X_{1a} Y_{1a} Z_{1a}$</p>	$\begin{pmatrix} u_{1e} \\ v_{1e} \\ w_{1e} \end{pmatrix} = \begin{pmatrix} e_{1xx} & e_{1xy} & e_{1xz} \\ e_{1yx} & e_{1yy} & e_{1yz} \\ e_{1zx} & e_{1zy} & e_{1zz} \end{pmatrix} \begin{pmatrix} u_e \\ v_e \\ w_e \end{pmatrix}$
<p>Step III</p> <p>$X_{1e} Y_{1e} Z_{1e} \rightarrow X_{1a} Y_{1a} Z_{1a}$</p>	$w_{1a} = (H - R_e w_{1e}) / (R_e^2 + H^2 - 2w_{1e} R_e H)$ $u_{1a} = v_{1e} (1 - w_{1a}^2)^{1/2} / (1 - w_{1e}^2)^{1/2}$ $v_{1a} = u_{1e} (1 - w_{1a}^2)^{1/2} / (1 - w_{1e}^2)^{1/2}$
<p>Step IV</p> <p>$X_{1a} Y_{1a} Z_{1a} \rightarrow X_a Y_a Z_a$</p>	$\begin{pmatrix} u_a \\ v_a \\ w_a \end{pmatrix} = \begin{pmatrix} a_{1xx} & a_{1yx} & a_{1zx} \\ a_{1xy} & a_{1yy} & a_{1zy} \\ a_{1xz} & a_{1yz} & a_{1zz} \end{pmatrix} \begin{pmatrix} u_{1a} \\ v_{1a} \\ w_{1a} \end{pmatrix}$

TABLE I.2-TRANSFORMATION OF COORDINATES FROM THE EARTH'S
COORDINATE SYSTEM TO THE ARRAY'S COORDINATE SYSTEM.

discussion. Thereby, the accomplishments listed below and illustrated in Figure I.3 will suffice to obtain an adequate set of transformation coefficients, i.e., to calibrate the system.

- (a) Determination of the direction cosines of the earth's center in the array coordinate system $(X_a Y_a Z_a)$; this gives the orientation of the Z_{1a} -axis in the array coordinate system.
- (b) Determination of the direction cosines of the array reference point in the earth's coordinate system $(X_e Y_e Z_e)$; this gives the orientation of the Z_{1e} -axis in the earth's coordinate system.
- (c) Determination of the direction cosines of an arbitrary point in space (the point can be located on the earth's surface) in both the array's and the earth's coordinate systems. This point (the point A in the figure) together with the array reference point and the earth's center will define the plane to be subtended by the Y-axis of the $X_{1a} Y_{1a} Z_{1a}$ coordinate system and the X-axis of the $X_{1e} Y_{1e} Z_{1e}$ coordinate system.

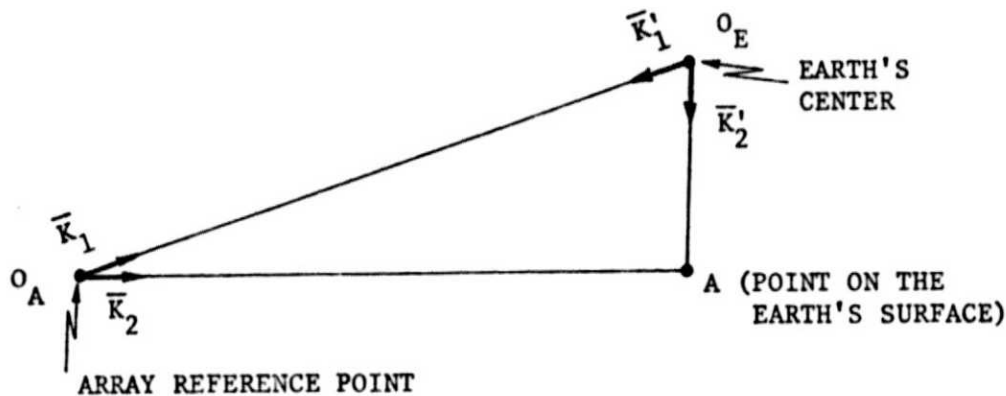


FIGURE I.1 UNIT VECTORS IN THE COORDINATE SYSTEMS OF THE ARRAY AND THE EARTH.

The transformation coefficients will then follow from

$$\begin{aligned}\bar{a}_{1z} &= \bar{k}_1 = a_{1zx}\bar{a}_x + a_{1zy}\bar{a}_y + a_{1zz}\bar{a}_z \\ \bar{a}_{1x} &= \frac{\bar{k}_2 \times \bar{k}_1}{|\bar{k}_2 \times \bar{k}_1|} = a_{1xx}\bar{a}_x + a_{1xy}\bar{a}_y + a_{1xz}\bar{a}_z \\ \bar{a}_{1y} &= \bar{k}_1 \times \frac{\bar{k}_2 \times \bar{k}_1}{|\bar{k}_2 \times \bar{k}_1|} = a_{1yx}\bar{a}_x + a_{1yy}\bar{a}_y + a_{1yz}\bar{a}_z\end{aligned}$$

and

$$\begin{aligned}\bar{e}_{1z} &= \bar{k}'_1 = e_{1zx}\bar{e}_x + e_{1zy}\bar{e}_y + e_{1zz}\bar{e}_z \\ \bar{e}_{1y} &= \frac{\bar{k}'_1 \times \bar{k}'_2}{|\bar{k}'_1 \times \bar{k}'_2|} = e_{1yx}\bar{e}_x + e_{1yy}\bar{e}_y + e_{1yz}\bar{e}_z \\ \bar{e}_{1x} &= \frac{\bar{k}'_1 \times \bar{k}'_2}{|\bar{k}'_1 \times \bar{k}'_2|} \times \bar{k}'_1 = e_{1xx}\bar{e}_x + e_{1xy}\bar{e}_y + e_{1xz}\bar{e}_z\end{aligned}$$

Therefore the only question is how to obtain the components of the vectors \bar{k}_1 , \bar{k}_2 , \bar{k}'_1 and \bar{k}'_2 in the corresponding coordinate systems.

One way to determine the components of the vectors \bar{k}_1 and \bar{k}_2 in the array coordinate system is to image the earth by a telescope mounted aboard the array. Namely, one can make use of the fact that known orientation of the telescope with respect to the array coordinate system and known characteristics of the optical system employed define a unique relationship between the direction cosines of the points in the object space in the array coordinate system and the position of the corresponding images in the image plane. Since the vector \bar{k}_1 by definition points toward the earth's center its components can be calculated from the position of the earth's disc in the image plane. Concerning the vector \bar{k}_2 we have in

principle the freedom to choose its orientation (or the values of its components in the array coordinate system) arbitrarily. However, in order to facilitate the determination of the components of the vector \bar{k}'_2 in the earth's coordinate system (\bar{k}'_2 by definition must lie in the same plane as \bar{k}_2) the following procedure should be followed. We pick up an arbitrary object on the earth's surface (small lake, small island, etc.) whose longitude and latitude are known and whose image can be identified in the image plane. Then, from the position of the object's image in the image plane we calculate the direction cosines of the object in the array coordinate system. Finally, we require the vector \bar{k}_2 to be pointed towards the object in question, i.e., we consider the calculated direction cosines as components of \bar{k}_2 .

The components of the vectors \bar{k}'_1 in the earth's coordinate system are specified by the longitude and the latitude of the array. (Methods exist by which the angular position of a geostationary satellite can be determined to within an rms uncertainty smaller than 0.1 milliradian [I.2]. This can be considered as quite satisfactory for the system we are concerned with.) The components of the vector \bar{k}'_2 are specified by the longitude and the latitude of the object which was used to define the vector \bar{k}_2 ; this object plays the role of the point A in Figure 13.

[I.2] A.M. McCaskill, D.V. Neil, and A.A. Satterlee, "Launch and Orbital Injection of Intelsat IV Satellites", COMSAT Technical Review, Volume 2, Number 2, Fall 1972.

APPENDIX II

DEPENDENCE OF THE UNCERTAINTY IN ANGULAR LOCATION ON THE BANDWIDTH
OF THE SYSTEM

Consider for simplicity a linear array with elements distributed along the x-axis which is focused at the point (u_0, f_0) in the uf -space. The complex factor $w(x)$ associated with the element at position x will then be given by

$$w(x) = e^{-j \frac{2\bar{u}}{c} f_0 u_0 x} \quad \text{II.1}$$

We want to locate the points (u, f) in the rf space for which the array response will be within the 3 dB limits as compared to its response to the point (u_0, f_0) . Since the normalized array response associated with an arbitrary point (u, f) is given by

$$\begin{aligned} O(u, f) &= \frac{1}{L} \int_x w(x) e^{j \frac{2\bar{u}}{c} f u x} dx \\ &= \frac{1}{L} \int_x e^{j \frac{2\bar{u}}{c} (f_u - f_0 u_0) x} dx \\ &= \frac{\sin\left\{\frac{\bar{f}}{c} L(f_u - f_0 u_0)\right\}}{\frac{\bar{f}}{c} L(f_u - f_0 u_0)} \end{aligned} \quad \text{II.2}$$

where L is the length of the array, all the points (u, f) satisfying

$$\left| \frac{\bar{f}}{c} L(f_u - f_0 u_0) \right| \leq 1.39 \quad \text{II.3a}$$

or

$$f_0 u_0 - \frac{1.39c}{\bar{f}L} \leq f_u \leq f_0 u_0 + \frac{1.39c}{\bar{f}L} \quad \text{II.3b}$$

will be within the 3 dB region. It is easy to see that this region will have the form depicted by the shaded area in Figure II.1.

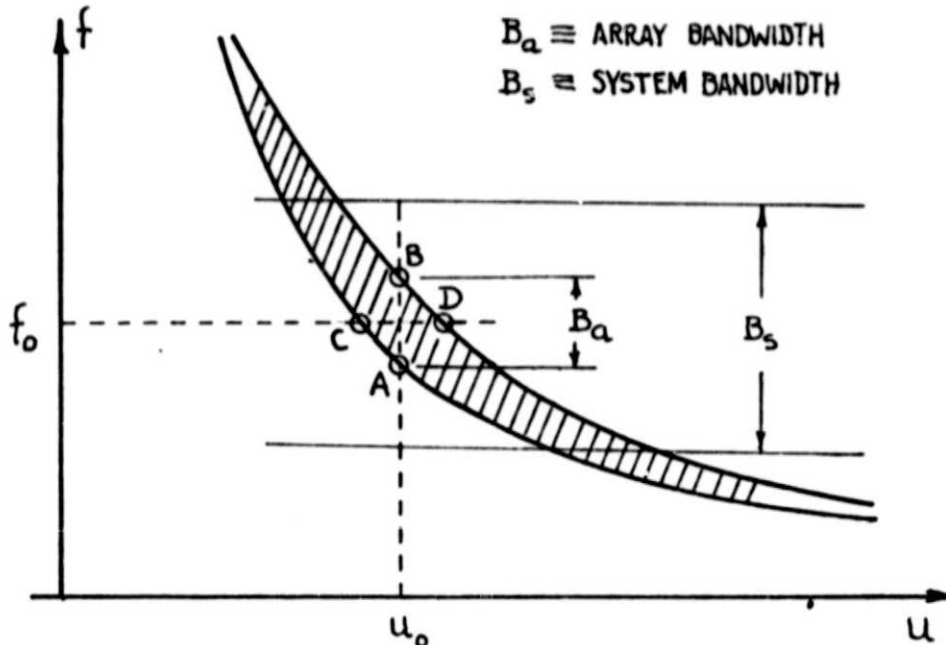


FIGURE II.1-SYSTEM'S BANDWIDTH - SINGLE
UNCERTAINTY RELATIONSHIP.

Observe that the distance between the points C and D corresponds to the array beamwidth and that the distance between the points A and B corresponds (and is numerically equal) to the array bandwidth B_u .

What one can conclude from the figure is the following. The uncertainty involved in determining the angular coordinate of a source detected is an increasing function of the uncertainty within which the frequency coordinate of the source was known. Since in practice the uncertainty associated with the frequency coordinate is given by the system's bandwidth (B_s , in the figure) one can also state that the uncertainty in angle is an increasing function of the system's bandwidth. Further, the

maximum error in angle determination equals $\gamma/2$ (half beamwidth) for $B_s \ll B_u$, it becomes equal to α (one beamwidth) for $B_s = B_u$ and rapidly increases with P_s when $B_s > B_u$.

ORIGINAL PAGE IS
OF POOR QUALITY